J. Non-Newtonian Fluid Mech. 166 (2011) 208–230

Contents lists available at ScienceDirect

Journal of Non-Newtonian Fluid Mechanics

journal homepage: www.elsevier.com/locate/jnnfm

Aspect ratio effects in laminar natural convection of Bingham fluids in rectangular enclosures with differentially heated side walls

Osman Turan[a,b], Robert J. Poole[a], Nilanjan Chakraborty[a,*]

[a] Department of Engineering, University of Liverpool, Brownlow Hill, Liverpool L69 3GH, UK
[b] Department of Mechanical Engineering, Karadeniz Technical University, Trabzon 61080, Turkey

ARTICLE INFO

Article history:
Received 16 September 2010
Received in revised form 8 November 2010
Accepted 4 December 2010
Available online 13 December 2010

Keywords:
Natural convection
Bingham fluids
Numerical simulation
Laminar flow

ABSTRACT

In this study, two-dimensional steady-state simulations of laminar natural convection in rectangular enclosures with differentially heated side walls have been conducted for a range of different aspect ratios AR (=H/L where H is the enclosure height and L is the enclosure width). The rectangular enclosures are considered to be completely filled with a yield-stress fluid obeying the Bingham model. Yield stress effects on heat and momentum transport are investigated for nominal values of Rayleigh number (Ra) in the range 10^4–10^6 and the aspect ratio range 1/8 to 8 for a single Prandtl number (Pr = 7). It is found that the mean Nusselt number $\overline{Nu}$ increases with increasing values of Rayleigh number for both Newtonian and Bingham fluids. However, $\overline{Nu}$ values obtained for Bingham fluids are smaller than that obtained in the case of Newtonian fluids with the same nominal value of Rayleigh number Ra due to weakening of convective transport. The mean Nusselt number $\overline{Nu}$ in the case of Bingham fluids is found to decrease with increasing Bingham number, and, for large values of Bingham number Bn, the value of $\overline{Nu}$ settles to unity (i.e. $\overline{Nu} = 1.0$) as heat transfer takes place principally due to thermal conduction. The effects of aspect ratio AR have also been investigated in detail and it has been found the effects of thermal convection (diffusion) strengthens (weakens) with increasing aspect ratio and *vice versa*, for a given set of nominal values of Rayleigh number Ra and Prandtl number Pr. It is found that the aspect ratio AR_{max} at which the maximum mean Nusselt number $\overline{Nu}$ occurs is found to decrease with increasing Rayleigh number. However, the value of AR_{max} is shown to increase with increasing Bingham number Bn for a given set of values of Ra and Pr. Detailed physical explanations are provided for the observed phenomena. New correlations are proposed for the mean Nusselt number $\overline{Nu}$ for Bingham fluids, which are shown to satisfactorily capture the correct qualitative and quantitative behaviour of $\overline{Nu}$ in response to changes in Ra, AR and Bn.

1. Introduction

Natural convection in rectangular enclosures is one of the most well-known problems of convective heat transfer and has several engineering applications such as in solar collectors, in heating and preservation of canned foods, in electronic equipment cooling and in energy storage and conservation. A lot of theoretical (e.g. Batchelor [1]), numerical (e.g. de Vahl Davis [2]) and experimental (e.g. Emery and Lee [3]) studies have been carried out for natural convection in rectangular enclosures filled with Newtonian fluids. An overview of the fundamental studies on this subject can be found in the review paper by Ostrach [4]. Although various different configurations of the enclosure problem are possible, one of the most studied cases involves two-dimensional enclosures where the horizontal walls are adiabatic and the temperature difference driving the convection comes from the side walls as in the classic benchmark paper of de Vahl Davies [2] for Newtonian fluids. To avoid unnecessary repetition, unless otherwise stated, all papers referred to in the remainder of the paper are concerned with this configuration. It has been found that the aspect ratio of the enclosure, defined as $AR = H/L$, in which H is the enclosure height and L is the enclosure width, has a major influence on the thermal transport in rectangular enclosures with differentially heated side walls [5–12].

The effects of aspect ratio on the natural convection in rectangular enclosures are often investigated separately for tall ($AR \gg 1$) and shallow enclosures ($AR \ll 1$). Elder [5] carried out a comprehensive experimental study on the natural convection in rectangular enclosures in the range of $Ra < 10^8$, $1 \leq AR \leq 60$ and $Pr = 1000$ (all dimensionless parameters are defined and discussed in Section 2.2). Elder [5] distinguished three regions; a region in the vicinity of vertical side walls where the temperature gradients are nearly horizontal and largest, an interior region where the vertical temperature gradients appear and an end region strongly influenced

* Corresponding author. Tel.: +44 1517944831; fax: +44 1517944848.
E-mail addresses: osmanturan@ktu.edu.tr (O. Turan), robpoole@liv.ac.uk (R.J. Poole), n.chakraborty@liv.ac.uk (N. Chakraborty).

0377-0257/$ – see front matter © 2010 Elsevier B.V. All rights reserved.
doi:10.1016/j.jnnfm.2010.12.002

Nomenclature

a	correlation parameter
AR	aspect ratio ($AR = H/L$)
b	correlation parameter
Bn	Bingham number
Bn^*	modified Bingham number for boundary-layer regime
Bn^{**}	modified Bingham number for parallel-flow regime
c_p	specific heat at constant pressure [J/kg K]
c_1, c_2, c_3	correlation parameter
C	correlation parameter
C_B	correlation parameter
e	relative error
f_1, f_2, f_3, f_4	functions relating thermal and hydrodynamic boundary layers
F	fraction determining the ratio of the hydrodynamic boundary layer thickness on horizontal surface to the height of the enclosure
g	gravitational acceleration [m/s^2]
Gr	Grashof number
h	heat transfer coefficient [W/m^2 K]
H	height of the enclosure [m]
k	thermal conductivity [W/m K]
K	thermal gradient in horizontal direction [K/m]
L	width of the enclosure [m]
m	stress growth exponent [s]
n, n_1, n_2	correlation parameter
n_B	exponent of aspect ratio for self similar variation of mean Nusselt number in the boundary-layer regime
Nu	Nusselt number
Nu_1	convective contribution to Nusselt number
Nu_2	conduction contribution to Nusselt number
$Nu_{Bn=0}$	Nusselt number for Newtonian fluids
Pr	Prandtl number
q	general quantity
q_e	correlation parameter
q_f	heat flux [W/m^2]
Ra	Rayleigh number based on L
Ra_H	Rayleigh number based on H.
T	temperature [K]
u_i, u_j	ith and jth velocity components [m/s]
U, V	dimensionless horizontal ($U = u_1 L/\alpha$) and vertical velocity ($V = u_2 L/\alpha$)
ϑ	characteristic velocity in vertical direction [m/s]
x_i, x_j	coordinate in ith and jth directions [m]

Greek letters

α	thermal diffusivity [m^2/s]
β	coefficient of thermal expansion [K^{-1}]
$\dot{\gamma}$	shear rate [s^{-1}]
δ, δ_{th}	hydrodynamic and thermal boundary layer thickness [m]
θ	dimensionless temperature, ($\theta = (T - T_C)/(T_H - T_C)$)
μ	plastic viscosity [N s/m^2]
μ_{yield}	yield viscosity [N s/m^2]
ν	kinematic viscosity [m^2/s]
ρ	density [kg/m^3]
τ_y	yield stres [N/m^2]
ϕ	general primitive variable
ψ	stream function [m^2/s]

Subscripts

C	cold wall
ext	extrapolated value
eff	effective value
H	hot wall
max	maximum value
ref	reference value
$wall$	wall value

Special characters

ΔT	difference between hot and cold wall temperature (=($T_H - T_C$)) [K]
ΔT_1	the temperature difference between the horizontal walls [K]
$\overline{Nu}$	mean Nusselt number
$\Delta_{\min,cell}$	minimum cell distance [m]
r_x, r_y	grid expansion ratio in x_1 and x_2 directions

by the boundary conditions. For $Ra < 10^3$, a weak, steady circulation in the flow is observed in the enclosure and the isotherms remain parallel to the vertical boundaries [5] and under this condition heat transfer takes place primarily due to conduction. For $10^3 < Ra < 10^5$, large temperature gradients appear near the walls and an almost uniform vertical temperature gradient establishes in the interior region. For large values of Ra, secondary and tertiary flows appear in the interior region of the flow. Bejan [9] proposed expressions for mean values of Nusselt number for tall enclosures which are in good agreement with experimental data [5]. Tall enclosures continue to be studied both experimentally and numerically [8,10,11–19] and interested readers are referred to Ganguli et al. [19] and references therein for an extensive review.

Shallow rectangular enclosures (i.e. $AR \ll 1$) were investigated analytically by Cormack et al. [20]. They considered the asymptotic problem in which $AR \to 0$ with constant Ra. It was highlighted that the flow structure consists of two distinct regimes which are namely the "parallel-flow" regime and the "boundary-layer" regime. In the parallel-flow regime two horizontal counter-currents are observed in the central core and the horizontal temperature gradient remains uniform throughout the central core with the isotherms parallel to the vertical walls. In contrast, in the boundary-layer regime the regions of high thermal gradients are confined to thin thermal boundary layers adjacent to the vertical walls and convection currents within the enclosure play a key role in thermal transport. Cormack et al. [20] obtained an expression for the mean Nusselt number based on an asymptotic analysis. An approximate criterion for the parallel-flow regime was given by $Ra^2\, AR^9 \leq 10^5$ based on their analysis (for $AR \sim 0.1$). In part II of their investigation Cormack et al. [21] numerically investigated the transition between parallel-flow and boundary-layer regimes for enclosures with aspect ratios AR ranging from 0.05 to 1 and the simulation results were compared with the asymptotic theory of Cormack et al. [20]. Cormack et al. [21] demonstrated that the parallel-flow regime appears with decreasing AR for a given value of Ra and the thermal boundary-layer structure transforms to a linear variation of temperature within the enclosure. The same situation occurred when Ra decreases for a given value of aspect ratio AR [21]. However, for high values of $Ra^2 AR^9$, the asymptotic theory [20] underestimates the Nusselt number obtained from the numerical simulations [21]. Bejan and Tien [22] proposed an alternative analytical method for predicting heat transfer in shallow enclosures. They developed a complete set of analytical results for Nusselt number corresponding to the three different regimes (parallel-flow regime, intermediate flow regime and boundary-layer regime,

which are discussed in Section 3 in detail) of convection in rectangular enclosures and it was demonstrated that their analysis satisfactorily predicts the mean Nusselt number obtained from numerical [21] and experimental [23] studies. Bejan et al. [25] established a limiting condition (i.e. $Ra > AR^{-7}$) for which convection begins to play an important role in thermal transport in enclosures with differentially heated side walls based on an experimental investigation involving a Newtonian fluid (i.e. water).

From the foregoing it is clear that rectangular enclosures with differentially heated side walls have been studied extensively for Newtonian fluids. In comparison limited effort has been devoted to the analysis of natural convection of non-Newtonian fluids in rectangular enclosures. As many synthetic fluids are non-Newtonian in character there are many practical applications where such effects will be important such as heating and preservation of canned foods (which are typically shear-thinning and often exhibit a yield stress).

For fluids exhibiting a yield stress, i.e. materials that behave as rigid solids for shear stresses lower than a critical yield stress but which flow for higher shear stresses, the paper of Vola et al. [26] and the recent paper of the present authors (Turan et al. [27]) are the only two papers that deal with natural convection of Bingham fluids in square enclosures with differentially heated vertical side walls. Vola et al. [26] developed a numerical method for simulating yield stress fluid flow obeying the Bingham model in a series of geometries. Their results show that as the yield stress is increased the strength of convection currents diminish and, as a consequence, the mean Nusselt number decreases. At high Bingham numbers convection is essentially absent from the flow and the heat transfer takes place solely by conduction. It was shown by Turan et al. [27] that the mean Nusselt number $\overline{Nu}$ increases with increasing Pr for Newtonian fluids and low Bingham number flows for a given value of the Rayleigh number. In contrast the opposite behaviour was observed for Bingham fluids for large values of the Bingham number. Moreover, in Turan et al. [27] computational data was used to propose correlations for the mean Nusselt number $\overline{Nu}$ for square cavities with heated side walls filled with both Newtonian and Bingham fluid in the range $10^3 < Ra < 10^6$ and $0.1 < Pr < 100$.

The effects of aspect ratio on the natural convection of yield stress fluids in rectangular enclosures with differentially heated side walls are yet to be analysed and the purpose of the current study is to address this void in the existing literature. In this respect the main objectives in the current work are as follows:

(1) To investigate yield stress effects on heat and momentum transport for nominal values of Rayleigh number in the range 10^4–10^6 and the aspect ratio range 1/8 to 8 for a single Prandtl number (i.e. $Pr = 7.0$). The primary focus of the current analysis is directed to the situation when flow within the enclosure is sufficient to alter the Nusselt number by a non-negligible amount. The situation where yielding first occurs – but the resulting flow velocities are too small to produce significant influence on thermal transport by convective heat transfer – is of only minor interest from the point of view of this study and this issue will not be significantly dwelt upon in this article.

(2) To produce an accurate correlation for the mean Nusselt number which captures the variations of mean Nusselt number in response to the changes in aspect ratio, Rayleigh, Prandtl and Bingham numbers.

2. Yield stress model, dimensionless paramaters and numerical method

2.1. Constitutive equation for yield stress fluid

Instead of entering into the ongoing debate about the very existence of a "true" yield stress, it is readily acknowledged that the notion of an apparent yield stress is an useful and practical engineering empiricism for a wide range of materials [28,29] and henceforth this concept will be adopted for the rest of the paper. A number of empirical models have been proposed for describing the shear rate dependence of shear stress in yield-stress fluids. The most well-known model is the Bingham model [28], which can be expressed in tensorial form in the following manner:

$$\underline{\underline{\dot{\gamma}}} = 0 \quad \text{for } \tau \le \tau_y, \tag{1}$$

$$\underline{\underline{\tau}} = \left(\mu + \frac{\tau_y}{\dot{\gamma}}\right)\underline{\underline{\dot{\gamma}}} \quad \text{for } \tau > \tau_y, \tag{2}$$

where $\dot{\gamma}_{ij} = \partial u_i/\partial x_j + \partial u_j/\partial x_i$ are the components of the rate of strain tensor $\underline{\underline{\dot{\gamma}}}$, $\underline{\underline{\tau}}$ the stress tensor, τ_y the yield stress, μ the so-called plastic viscosity of the yielded fluid, τ and $\dot{\gamma}$ are evaluated based on the second invariants of the stress and the rate of strain tensors respectively (in a pure shear flow), which can be defined as:

$$\tau = \left[\frac{1}{2}\underline{\underline{\tau}} : \underline{\underline{\tau}}\right]^{1/2}, \tag{3}$$

$$\dot{\gamma} = \left[\frac{1}{2}\underline{\underline{\dot{\gamma}}} : \underline{\underline{\dot{\gamma}}}\right]^{1/2}. \tag{4}$$

O'Donovan and Tanner [30] used the bi-viscosity model to mimic the stress-shear rate characteristics for a Bingham fluid in the following manner:

$$\underline{\underline{\tau}} = \mu_{yield}\underline{\underline{\dot{\gamma}}} \quad \text{for } \dot{\gamma} \le \frac{\tau_y}{\mu_{yield}}, \tag{5a}$$

$$\underline{\underline{\tau}} = \tau_y + \mu\left[\underline{\underline{\dot{\gamma}}} - \frac{\tau_y}{\mu_{yield}}\right] \quad \text{for } \dot{\gamma} > \frac{\tau_y}{\mu_{yield}}, \tag{5b}$$

where μ_{yield} is the yield viscosity. In effect this GNF model replaces the solid material by a fluid of high viscosity. O'Donovan and Tanner [30] showed that a value of μ_{yield} equal to 1000μ mimics the true Bingham model in a satisfactory way. To investigate the effect of the current choice of regularisation some limited simulations have also been conducted using the exponential model due to Papanastasiou [31]

$$\underline{\underline{\tau}} = \tau_y(1 - e^{-m\dot{\gamma}}) + \mu\underline{\underline{\dot{\gamma}}}, \tag{6}$$

where m is the stress growth exponent which has the dimensions of time. Again this model transforms the "solid" region to a viscous one of high viscosity.

2.2. Dimensionless numbers

The Rayleigh number Ra represents the ratio of the strengths of thermal transports due to buoyancy to thermal conduction, which is defined in the present study as:

$$Ra = \frac{\rho^2 c_p g\beta\Delta T L^3}{\mu k} = GrPr, \tag{7}$$

where Gr is the Grashof number and Pr is the Prandtl number, which are defined as:

$$Gr = \frac{\rho^2 g\beta\Delta T L^3}{\mu^2} \quad \text{and} \quad Pr = \frac{\mu c_p}{k}. \tag{8}$$

The Grashof number represents the ratio of the strengths of buoyancy and viscous forces while the Prandtl number depicts the ratio of momentum diffusion to thermal diffusion. Alternatively, the Prandtl number can be taken to represent the ratio of the hydrodynamic boundary layer to thermal boundary layer thicknesses.

These definitions are referred to as "nominal" values as they contain the constant plastic viscosity μ (i.e. are not based on a viscosity representative of the flow). Using dimensional analysis it is possible to show that for Bingham fluids: $Nu = f_1(Ra, Pr, Bn, AR)$ where the Nusselt number Nu and Bingham number Bn are given by:

$$Nu = \frac{hL}{k} \quad \text{and} \quad Bn = \frac{\tau_y}{\mu}\sqrt{\frac{L}{g\beta\Delta T}}, \tag{9}$$

where Nu represents the ratio of heat transfer rate by convection to that by conduction in the fluid in question and the heat transfer coefficient h is defined as:

$$h = \left| -k \left.\frac{\partial T}{\partial x_1}\right|_{wf} \times \frac{1}{(T_{wall} - T_{ref})} \right|, \tag{10}$$

where subscript 'wf' refers to the condition of the fluid in contact with the wall, T_{wall} is the wall temperature and T_{ref} is the appropriate reference temperature, which can be taken to be T_C (T_H) for the hot (cold) wall respectively. As the viscosity varies throughout the Bingham fluid flow, an effective viscosity expressed as $\mu_{eff} = \tau_y/\dot{\gamma} + \mu$ might be more representative of the viscous stress within the flow than the constant plastic viscosity μ [27]. Therefore the Rayleigh, Prandtl and Bingham numbers could have been defined more appropriately if μ_{eff} was used instead of μ. However $\dot{\gamma}$ is expected to show local variations in the flow domain so using a single characteristic value in the definitions of the dimensionless numbers may not yield any additional benefit in comparison to the definitions given by Eqs. (7)–(9), although the concept is useful in explaining some observed phenomena as discussed in Turan et al. [27]. Here the results will be confined to a single Prandtl number, $Pr = 7$, which is representative of an incompressible fluid such as water. Although many fluids may have larger values of Pr than this value, previous results [cf. Fig. 8 in Ref. [27]] by the present authors indicate that above this value any effects of Pr are rather small for Newtonian fluids: for a square enclosure at $Ra = 10^3$ and $Ra = 10^4$ the Nusselt number for $Pr = 100$ is the same as $Pr = 7$ to 3 d.p, at $Ra = 10^5$ and $Ra = 10^6$ the difference is less than 0.1%.

It is important to note that in the present study the plastic viscosity μ and yield stress τ_y are taken to be independent of temperature. The rationale behind this choice is discussed in detail in a previous paper (Ref. [27]) by the present authors.

2.3. Numerical method

A commercial finite-volume code (FLUENT) is used to solve the coupled conservation equations of mass, momentum and energy. The numerical method followed in this study is similar to that adopted in a number of recent studies for both inelastic power-law [32] and Bingham [33,34] fluids. In this framework, a second-order central differencing scheme is used for the diffusive terms and a second-order up-wind scheme for the convective terms. Coupling of the pressure and velocity is achieved using the well-known SIMPLE (Semi-Implicit Method for Pressure-Linked Equations) algorithm [35]. The convergence criteria were set to 10^{-9} for all the relative (scaled) residuals.

2.3.1. Governing equations

For the present study steady-state flow of an incompressible Bingham fluid is considered. For incompressible fluids the conservation equations for mass, momentum and energy under steady state can be written in the following manner using tensor notation:

Mass conservation equation

$$\frac{\partial u_i}{\partial x_i} = 0, \tag{11}$$

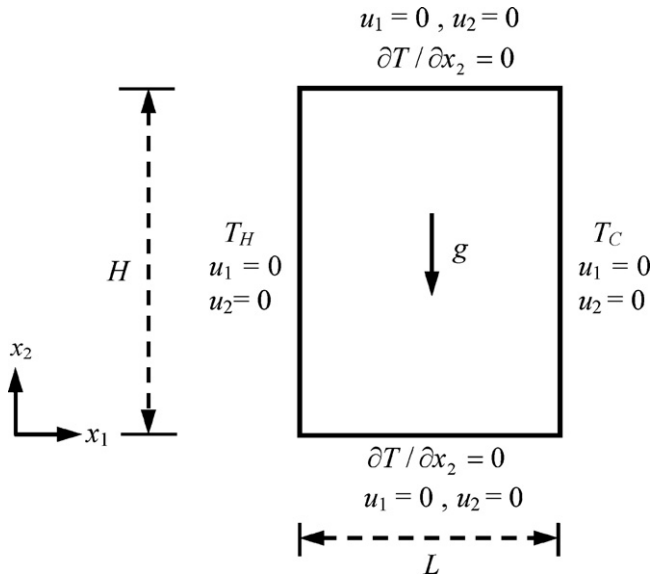

Fig. 1. Schematic diagram of the simulation domain.

Momentum conservation equations

$$\rho u_j \frac{\partial u_i}{\partial x_j} = -\frac{\partial p}{\partial x_i} + \rho g \beta \delta_{i2}(T - T_C) + \frac{\partial \tau_{ij}}{\partial x_j}, \tag{12}$$

Energy conservation equation

$$\rho u_j c_p \frac{\partial T}{\partial x_j} = \frac{\partial}{\partial x_j}\left(k \frac{\partial T}{\partial x_j}\right), \tag{13}$$

where x_1 and x_2 co-ordinates (i.e. $x_1 = x$ and $x_2 = y$) are taken along the horizontal and vertical directions respectively, the cold wall temperature T_C is taken to be the reference temperature for evaluating the buoyancy term $\rho g \delta_{i2} \beta (T - T_C)$ (where δ_{i2} is the component of Kronecker's delta δ_{ij} so that the term $\rho g \delta_{i2} \beta (T - T_C)$ remains operational only in the x_2 direction) are in the momentum conservation equations following several previous studies [2,11–21,26,27].

The bi-viscosity model [30] (see Eqs. (5a) and (5b)) is used to model the viscous effects of the Bingham fluid in this study. Buoyancy effects are accounted for by Boussinesq's approximation but the fluid properties are otherwise assumed to be temperature-independent. The ratio of the yield viscosity (μ_{yield}) to the plastic viscosity (μ) was set to 10^4. In order to assess the sensitivity of the μ_{yield} value, the simulations have been carried out for both $\mu_{yield} = 10^3\,\mu$ and $\mu_{yield} = 10^4\,\mu$ and quantitative agreement between the results are found to be satisfactory (i.e. maximum deviation in $\overline{Nu}$ is of the order of 3%, which is still much smaller than the experimental uncertainty in the present configuration) for all the cases. Given this agreement only results corresponding to $\mu_{yield} = 10^4\,\mu$ are presented in this paper.

2.3.2. Boundary conditions

The simulation domain is shown schematically in Fig. 1 where the two vertical walls of a rectangular enclosure are kept at different temperatures ($T_H > T_C$), whereas the other boundaries are considered to be adiabatic in nature. The velocity components (i.e. $u_1 = u$ and $u_2 = v$) are identically zero on each boundary because of the no-slip condition and impenetrability of rigid boundaries. The temperatures for cold and hot vertical walls are specified (i.e. $T(x_1 = 0) = T_H$ and $T(x_2 = L) = T_C$). The temperature boundary

Table 1
Minimum cell distances ($\Delta x_{min,cell}/L$, $\Delta y_{min,cell}/H$) and grid expansion ratios (r_x, r_y) values.

	Grid	M1 40 × 40	M2 80 × 80	M3 160 × 160
$AR = 0.125$	$\Delta x_{min,cell}/L$	–	8.7848×10^{-4}	–
	r_x	–	1.1092	–
	$\Delta y_{min,cell}/H$	–	7.0278×10^{-4}	–
	r_y	–	1.0274	–
$AR = 0.25$	$\Delta x_{min,cell}/L$	–	8.7848×10^{-4}	–
	r_x	–	1.1092	–
	$\Delta y_{min,cell}/H$	–	3.5139×10^{-3}	–
	r_y	–	1.0566	–
$AR = 0.5$	$\Delta x_{min,cell}/L$	1.8534×10^{-3}	8.7848×10^{-4}	4.3001×10^{-4}
	r_x	1.2303	1.1092	1.0532
	$\Delta y_{min,cell}/H$	3.6608×10^{-3}	1.7570×10^{-3}	8.6086×10^{-4}
	r_y	1.1741	1.0836	1.0409
$AR = 1$	$\Delta x_{min,cell}/L$	–	8.7848×10^{-4}	–
	r_x	–	1.1092	–
	$\Delta y_{min,cell}/H$	–	8.7848×10^{-4}	–
	r_y	–	1.1092	–
	Grid	M2 80 × 80	M4 80 × 160	M5 80 × 320
$AR = 2$	$\Delta x_{min,cell}/L$	–	8.7848×10^{-4}	–
	r_x	–	1.1092	–
	$\Delta y_{min,cell}/H$	–	4.3924×10^{-4}	–
	r_y	–	1.0532	–
$AR = 4$	$\Delta x_{min,cell}/L$	8.7848×10^{-4}	8.7848×10^{-4}	8.7848×10^{-4}
	r_x	1.1092	1.1092	1.1092
	$\Delta y_{min,cell}/H$	8.7848×10^{-4}	4.2750×10^{-4}	2.1962×10^{-4}
	r_y	1.1092	1.0532	1.0262
$AR = 8$	$\Delta x_{min,cell}/L$	–	8.7848×10^{-4}	–
	r_x	–	1.1092	–
	$\Delta y_{min,cell}/H$	–	5.4905×10^{-5}	–
	r_y	–	1.0371	–

conditions for the horizontal insulated boundaries are given by: $\partial T/\partial x_2 = 0$ at $x_2 = 0$ and $x_2 = H$.

2.3.3. Grid independency study

The grid independence of the results has been established based on a careful analysis of five different non-uniform meshes M1 (40×40), M2 (80×80), M3 (160×160), M4 (80×160) and M5 (80×320) and the details of these grids are included in Table 1. For $AR \leq 1$ (M1–M2–M3) and for $AR > 1$ (M2–M4–M5) different meshes were used to assess the numerical uncertainty. For some representative simulations (Newtonian ($Bn = 0$) and $Bn = 1$ for $Ra = 10^6$ and $Pr = 7$ for $AR = 0.5$ and 4) the numerical uncertainty is quantified here using Richardson's extrapolation theory [36]. For a primitive variable ϕ the Richardson's extrapolation value is given by: $\phi_{h=0} = \phi_1 + (\phi_2 - \phi_1)/(r^p - 1)$ where ϕ_1 is obtained based on fine grid and ϕ_2 is the solution based on next level of coarse grid, r is the ratio between coarse to fine grid spacings and p is the theoretical order of accuracy. In this analysis the apparent order p was taken to be 2. The numerical uncertainties for the mean Nusselt number $\overline{Nu}$ and the maximum vertical velocity (V_{max}) magnitude on the horizontal mid-plane of the enclosure are presented in Table 2. As seen in Table 2, the numerical uncertainty levels between meshes are less than 1% for mean $\overline{Nu}$ and V_{max} in both aspect ratio cases. Based on these uncertainties, mesh M2 was used for $AR \leq 1$, mesh M4 used for $AR = 2$ and mesh M5 was used for $AR = 4$ and 8. In addition to this grid-dependency study, the simulation results for square enclosures filled with Newtonian and Bingham fluids were compared with the benchmark data of de Vahl Davis [2] and Vola et al. [26] respectively and the agreement between the results was found to be very good and entirely consistent with the aforementioned grid-dependency studies. Interested readers are referred to Turan et al. [27] for further details on benchmarking of present simulation results.

3. Convection regimes and existing correlations

Bejan and Tien [22] identified three different laminar convection regimes in Newtonian fluids for rectangular enclosures with differentially heated sidewalls. Under the condition when $Ra_H = \rho g \beta (T_H - T_C) H^3/\mu\alpha = Ra\,AR^3$ approaches to zero (i.e. $RaAR^3 \to 0$) the vertical velocity component at the core of the enclosure disappears and flow in the box consists mainly of two horizontal counter currents and the temperature gradient in the horizontal direction remains constant throughout the core of the enclosure. This regime will henceforth be referred to as the 'parallel-flow regime'. Cormack et al. [20] carried out asymptotic analysis for the $RaAR^3 \to 0$ limit and obtained the following expression for the mean Nusselt number (i.e. $\overline{Nu} = \int_0^H Nu\, dx_2/H$):

$$\overline{Nu} = 1 + \frac{Ra^2 AR^8}{362880}. \tag{14}$$

The temperature difference between the horizontal walls ΔT_1 in the $RaAR^3 \to 0$ limit is given by [20]:

$$\Delta T_1 = RaAR^5 \frac{(T_H - T_C)}{720}. \tag{15}$$

Bejan and Tien [22] argued that $\Delta T_1 \leq (T_H - T_C)/10$ in the parallel-flow regime (i.e. $RaAR^3 \to 0$) which yields the following criterion for this regime:

$$Ra < 72(AR)^{-5}. \tag{16}$$

The other extreme convection condition is referred to as the 'boundary-layer regime' by Bejan and Tien [22] where Ra assumes

Table 2
Numerical uncertainty for mean Nusselt number $\overline{Nu}$ and maximum vertical velocity component V on the horizontal mid-plane (i.e. $y/H = 0.5$) at $Ra = 10^6$ and $Pr = 7$ for Newtonian and Bingham ($Bn = 1$) fluids for $AR = 0.5$ and 4.

$AR = 0.5$		$\overline{Nu}$			V_{max}		
		M1	M2	M3	M1	M2	M3
Newtonian fluid	ϕ	9.192	9.223	9.238	168.812	170.928	171.449
	ϕ_{ext}		9.243			171.620	
	e_{ext} (%)	0.548	0.211	0.053	1.638	0.405	0.101
Bingham fluid ($Bn = 1$)	ϕ	6.194	6.228	6.242	78.991	79.210	79.469
	ϕ_{ext}		6.247			79.555	
	e_{ext} (%)	0.843	0.299	0.074	0.709	0.434	0.109
$AR = 4$		$\overline{Nu}$			V_{max}		
		M2	M4	M5	M2	M4	M5
Newtonian fluid	ϕ	7.203	7.212	7.217	465.024	466.251	466.520
	ϕ_{ext}		7.222			466.790	
	e_{ext} (%)	0.263	0.138	0.069	0.378	0.115	0.058
Bingham fluid ($Bn = 1$)	ϕ	6.464	6.471	6.475	350.920	352.994	353.091
	ϕ_{ext}		6.479			353.190	
	e_{ext} (%)	0.231	0.123	0.061	0.642	0.055	0.027

large values and ΔT_1 remains comparable to $\Delta T = (T_H - T_C)$ (i.e. $\Delta T_1 \sim \Delta T$). Under this condition, high values of temperature gradient are confined to two thin boundary layers adjacent to the vertical walls. Bejan and Tien [22] obtained the following correlation for the boundary-layer regime:

$$\overline{Nu} = 0.623 Ra^{1/5} AR^{-2/5}. \tag{17}$$

In this regime the horizontal temperature gradient is given by:

$$K = \frac{\partial T}{\partial x_1} \sim 60.93 Ra^{3/5} AR^{9/5} \frac{\Delta T}{H}. \tag{18}$$

Bejan and Tien [22] argued that the inception of the boundary-layer regime can be indicated by $K < 0.1(\Delta T/L)$ which gives rise to the following criterion:

$$Ra > 4.4 \times 10^4 AR^{-14/3}. \tag{19}$$

Some of the characteristics of both the boundary layer and $RaAR^3 \to 0$ regimes are observed if the Rayleigh number Ra falls in the range:

$$72(AR)^{-5} < Ra < 4.4 \times 10^4 AR^{-14/3}. \tag{20}$$

Bejan and Tien [22] termed this as the 'intermediate regime'. Bejan and Tien [22] combined Eqs. (14) and (17) to come up with the following correlation which can be applied for all the three aforementioned regimes:

$$\overline{Nu} = 1 + \left[\left(\frac{Ra^2 AR^8}{362880} \right)^n + (0.623 Ra^{1/5} AR^{-2/5})^n \right]^{1/n}, \quad \text{where } n = -0.386 \tag{21}$$

Berkovsky and Polevikov [37] proposed the following correlation for square enclosures including Prandtl number effects:

$$\overline{Nu} = 0.18 \left(\frac{RaPr}{0.2 + Pr} \right)^{0.29}. \tag{22}$$

Recently the present authors proposed a new correlation [27] which was shown to provide better agreement with the predictions of numerical simulations [27,38] than the correlation proposed by Berkovsky and Polevikov [27]:

$$\overline{Nu} = 0.162 Ra^{0.293} \left(\frac{Pr}{1 + Pr} \right)^{0.091}. \tag{23}$$

For tall enclosures (i.e. $AR \gg 1$ but in practice usually $20 > AR > 2$) the mean Nusselt number is often expressed as: $\overline{Nu} = c_1 Ra^{c_2} AR^{c_3}$ and Bejan's analysis [9] demonstrated that the constants c_1, c_2 and c_3 are functions of Ra and AR. Bejan [9] also showed that the analytical results of Gill [6] leads to the following expression of $\overline{Nu}$ for extremely large values of aspect ratio (i.e. $Ra^{1/7} AR \to \infty$):

$$\overline{Nu} = 0.364 [Ra/(PrAR)]^{1/4}. \tag{24}$$

According to Bejan [9] $\overline{Nu}$ for tall enclosures is given by:

$$\overline{Nu} = C_B \left[\frac{Ra}{PrAR} \right]^{1/4} \int_{-q_e}^{q_e} \frac{(1-q)^6 (1+q)^2 (7-q^2)}{(1+q^2)(1+3q^2)^{14/3}} \, dq, \tag{25}$$

where C_B and q_e are functions of $Ra^{1/7} AR$ and C_B (q_e) is found to decrease (increase) from 1.0 to 0.912 (0.1 to 1.0) with an increase in $Ra^{1/7} AR$ from 0 to 1000 [9]. Bejan [9] found that $\overline{Nu}$ for tall enclosures deviate from the asymptotic value when $Ra^{1/7} AR < 100$ and the prediction of Eq. (25) approaches to that of Eq. (24) for $(Ra/AR)^{1/4} \geq 10$.

Different mean Nusselt number correlations have been proposed for tall enclosures based on experimental [8,10,12] and computational [11,13–19] studies and interested readers are referred to Ganguli et al. [19] for an extensive review and the assumptions behind the respective correlations. One of the most used correlations for tall enclosures with $AR > 5$ was proposed by Elsherbiny et al. [10]:

$$\overline{Nu} = Max(Nu_{1c}, Nu_{2c}, N_{3c}), \tag{26a}$$

where Nu_{1c}, Nu_{2c} and Nu_{3c} are given by:

$$Nu_{1c} = 0.0605 Ra^{1/3}; \quad Nu_{2c} = \left[1 + \left[\frac{0.104 Ra^{0.293}}{1 + (6310/Ra)^{1.36}} \right]^3 \right]^{1/3} \quad \text{and} \quad Nu_{3c} = 0.242 \left(\frac{Ra}{AR} \right)^{0.272} \tag{26b}$$

Natural convection of Bingham fluids in rectangular enclosures with differentially heated vertical side walls have been rarely studied hitherto but recently the present authors (Turan et al. [27])

Table 3
Variations of mean Nusselt number ($\overline{Nu}$) with aspect ratio (AR) in the case of Newtonian fluids for $Ra = 10^4 - 10^6$ and $Pr = 7$.

Ra	AR						
	0.125	0.25	0.50	1	2	4	8
10^4	1.0000[a]	1.0000[a]	1.2942[b]	2.2742[b]	2.3894[c]	2.1781[c]	1.8437[c]
10^5	1.0014[a]	1.2429[b]	3.8490[b]	4.7217[c]	4.4895[c]	3.9799[c]	3.4426[c]
10^6	1.1345[a]	5.6085[b]	9.2232[b]	9.2218[c]	8.3235[c]	7.2224[c]	6.1594[c]

[a] Parallel-flow regime ($RaAR^3 \to 0$).
[b] Intermediate regime.
[c] Boundary-layer regime.

proposed the following expression of $\overline{Nu}$ for square enclosures:

$$\overline{Nu} = 1 + \frac{ARa^{1/2}}{\left[Bn/2 + 1/2\sqrt{Bn^2 + 4(Ra/Pr)^{1/2}}\right]}\left[1 - \frac{Bn}{Bn_{\max}}\right]^b, \quad (27a)$$

where A, b and Bn_{max} are given by:

$$A = 0.162Ra^{0.043}\frac{Pr^{-0.159}}{(1+Pr)^{0.091}} - \frac{1}{Ra^{0.25}Pr^{0.25}};$$

$$b = 0.42Ra^{0.13}Pr^{0.12}; Bn_{\max} = 0.019Ra^{0.56}Pr^{-0.46}. \quad (27b)$$

The prediction of Eq. (27) was shown to be in good agreement with numerical simulation results for $Ra = 10^3$–10^6 and $Pr = 0.1$–100 in Turan et al. [27]. The correlation given by Eq. (27) will be extended to incorporate aspect ratio effects in the next section of this paper.

4. Results and discussion

4.1. Rayleigh number effects

Variations of mean Nusselt number $\overline{Nu}$ with AR for Newtonian fluids at Rayleigh numbers $Ra = 10^4$, 10^5 and 10^6 are provided in Table 3. The convection regimes according to Eqs. (16), (19) and (20) for the cases considered here are also indicated in Table 3. It can be seen from Table 3 that most $AR \geq 1$ cases for Rayleigh number $Ra = 10^4$, 10^5 and 10^6 belong to the boundary-layer regime except for the $AR = 1.0$ case at $Ra = 10^4$, which belongs to the intermediate flow regime. Table 3 further indicates that all the $AR < 1$ cases considered here represent either the parallel-flow regime or the intermediate flow regime. The distributions of temperature θ and vertical velocity component V with the normalised distance (i.e. x/L) along the horizontal mid-plane (i.e. $y/H = 0.5$) for Newtonian fluids are shown in Fig. 2a–c for Rayleigh number $Ra = 10^4$, 10^5 and 10^6 respectively at different values of aspect ratio AR ranging from 0.125 to 8.0. In Fig. 2a-c the distribution of θ remains linear for small values of aspect ratio (e.g. $AR = 0.125$) for $Ra = 10^4$, 10^5 and 10^6 where the flow in these cases corresponds to the parallel-flow regime. This linear temperature profile essentially indicates conduction-driven thermal transport, which is consistent with the expected behaviour in the parallel-flow regime [20–22]. Under pure conduction the temperature distribution along the x direction can be determined analytically and follows $d^2T/dx^2 = 0$ which, along with the given temperature boundary conditions, results in a linear temperature variation along the x direction. The conduction-dominated thermal transport is reflected by the $\overline{Nu}$ values reported in Table 3, which shows that $\overline{Nu}$ assumes values close to unity for the cases belonging to the parallel-flow regime. In the $Ra = 10^6$ case the distribution of θ at $AR = 0.25$ exhibits a linear variation for the major part of the enclosure except close to the vertical wall where the temperature distribution shows a change in slope characteristic of a thermal boundary layer, whereas a linear variation of θ is observed for $AR = 0.25$ for $Ra = 10^4$ and 10^5. For $Ra = 10^4$ and 10^5 the flow within the enclosure for $AR = 0.25$ represents the parallel-flow regime whereas the flow for $Ra = 10^6$ in the enclosure with $AR = 0.25$ belongs to the intermediate flow regime. As a result of this, the distribution of θ at $AR = 0.25$ for $Ra = 10^6$ shows some attributes of both the parallel-flow and boundary-layer regimes. It can be seen from Fig. 2a–c that the temperature θ distribution becomes non-linear for higher values of AR for all the values of Ra considered here and this distribution essentially indicates thermal boundary layers adjacent to the hot and cold walls and an almost isothermal core at the centre of the enclosure. The steepness of the temperature profile close to the vertical walls essentially determines the heat transfer rate and the maximum value of $\overline{Nu}$ is obtained for the aspect ratio at which the temperature gradient is the steepest in this near-wall region. However, the steepness of the temperature distribution close to the vertical walls does not exhibit any monotonic trend with aspect ratio. The steepness of the temperature profile close to the vertical wall increases with increasing aspect ratio until a value of aspect ratio $AR_{\max}$ is reached for which the maximum value of $\overline{Nu}$ is obtained. The steepness of the temperature distribution near the vertical walls and the mean Nusselt number $\overline{Nu}$ decrease with increasing aspect ratio when the aspect ratio exceeds $AR_{\max}$ (i.e. $AR > AR_{\max}$). A comparison between Fig. 2a–c reveals that the value of $AR_{\max}$ decreases with increasing Rayleigh number Ra, which is consistent with previous studies [18,19,24].

It is instructive to examine the distributions of vertical velocity component in order to understand and explain the observations made from temperature θ distributions. Fig. 2a–c indicate that the magnitude of V increases monotonically with increasing Ra for a given value of AR. Moreover, the magnitude of V increases with AR when Ra is held constant. Comparison of θ and V distributions in Fig. 2a-c reveals that V values for the cases where the parallel-flow regime occurs are essentially negligible (see Table 3), which is again consistent with the assumptions made for the analysis of the flows belonging to the parallel-flow regime by several previous studies [20–22]. These trends essentially indicate that the effects of convection in the enclosure strengthen with increasing aspect ratio AR. The value of Rayleigh number for which convection starts to play an important role is given by $Ra > AR^{-7}$ according to the criterion proposed by Bejan et al. [25] and this criterion suggests that the Rayleigh number above which convection effects become important in the thermal transport for $AR = 0.125$, 0.25 and 0.5 cases are of the order of 10^6, 10^4 and 10^2 respectively. This criterion, in conjunction with the data shown in Table 3 and Fig. 2a–c, suggests that convective effects and boundary layer transport have important influences on thermal transport for the aspect ratio values close to $AR_{\max}$ for the cases considered here. The non-monotonic aspect ratio dependence of mean Nusselt number can be explained based on a scaling analysis of the boundary-layer regime flow where the zones of high temperature gradient are confined close to the vertical walls (i.e. as in Fig. 2a–c). Under this situation the equilibrium of inertial and buoyancy forces in the boundary layer adjacent to the vertical walls yields:

$$\rho\frac{\vartheta^2}{H} \sim \rho g\beta\Delta T \quad \text{or} \quad \vartheta \sim \sqrt{g\beta\Delta TH}. \quad (28)$$

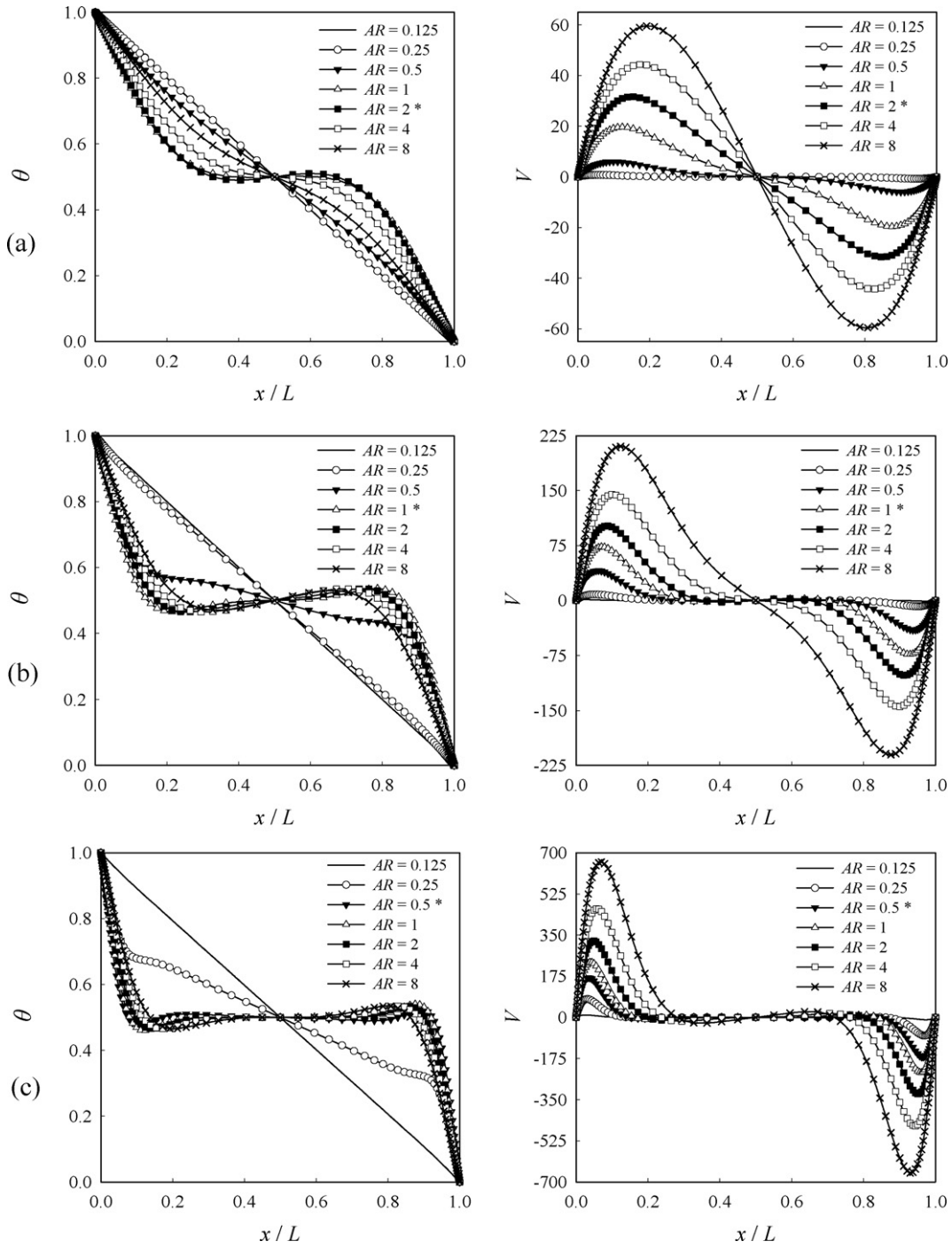

Fig. 2. Variations of temperature θ and vertical velocity component V along the horizontal mid-plane (i.e. $y/H = 0.5$) for Newtonian fluid case at $Pr = 7$: (a) $Ra = 10^4$, (b) $Ra = 10^5$ and (c) $Ra = 10^6$ (asterisk (*) highlights the AR in which the maximum mean Nusselt number $\overline{Nu}$ occurs).

Eq. (28) indicates that the vertical velocity component V scales as:

$$V \sim \frac{\vartheta L}{\alpha} \sim \sqrt{RaPrAR} \tag{29}$$

In the present study α/L is held constant for all the cases and thus Eq. (29) suggests that the effects of fluid flow strengthen with increasing AR (Ra) when $Ra(AR)$ is held constant i.e. entirely consistent with the observations made from Fig. 2a–c. For the purpose of understanding the non-monotonic behaviour of $\overline{Nu}$ with AR it is useful to consider the equilibrium of viscous and inertial forces, which yields:

$$\rho \frac{\vartheta^2}{H} \sim \mu \frac{\vartheta}{\delta^2} \quad \text{or} \quad \delta \sim \sqrt{\frac{\mu H}{\rho \vartheta}}. \tag{30a}$$

Using Eq. (28) in Eq. (30a) yields:

$$\delta \sim L(AR)^{0.25} \left(\frac{Pr}{Ra}\right)^{0.25} \tag{30b}$$

Based on the definition of Prandtl number one obtains $\delta/\delta_{th} = f_1(\mathrm{Pr})$ where $f_1(Pr)$ is a function which increases with increasing Pr. Using Eqs. (28)–(30) the advection terms $\rho c_p u_j \partial T/\partial x_j$ and

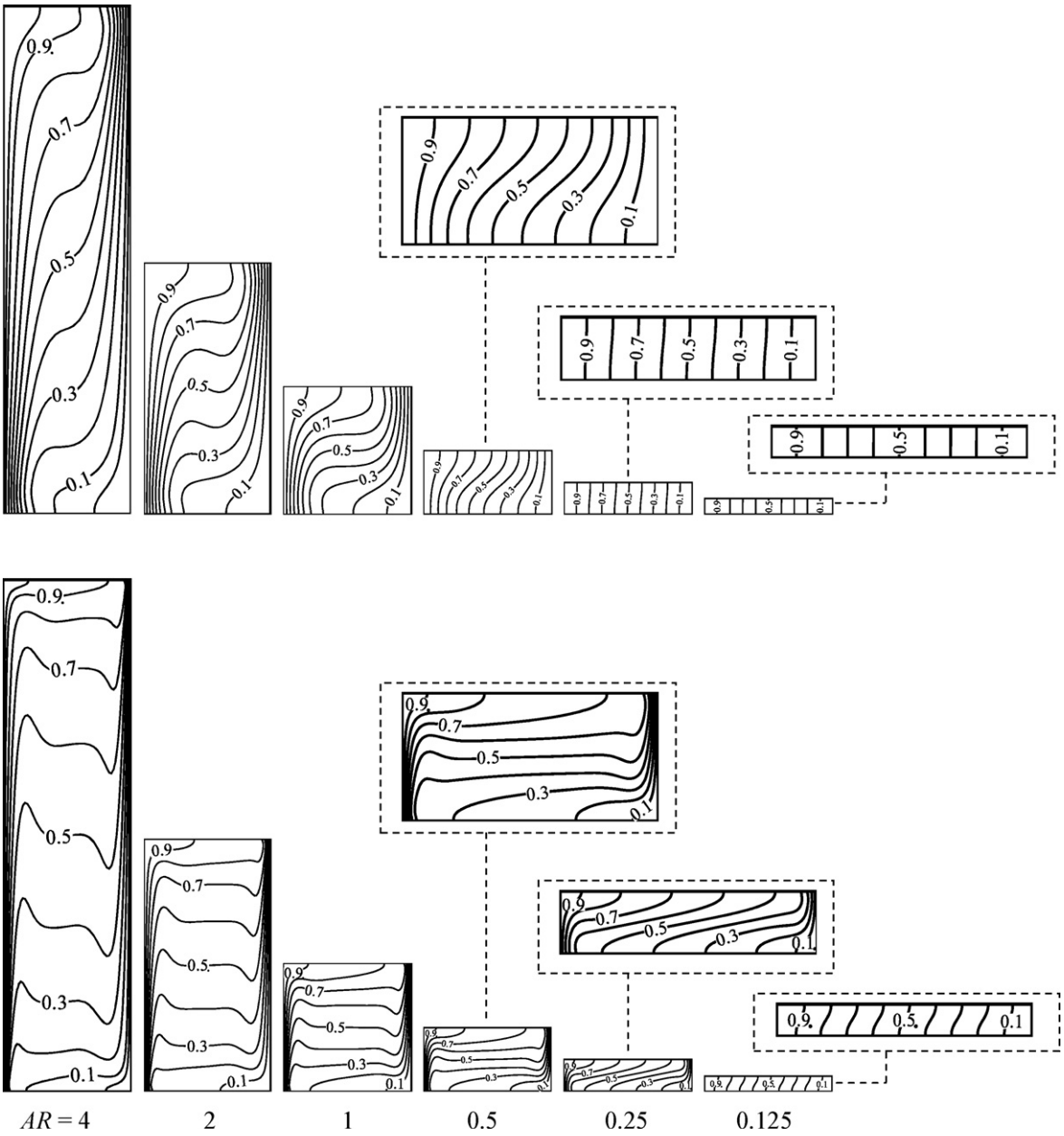

Fig. 3. Contours of temperature θ for convection in Newtonian fluids at $Pr = 7$ for $Ra = 10^4$ (1st row) and $Ra = 10^6$ (2nd row).

the thermal diffusion (i.e. conduction) terms $\nabla.(k\nabla T)$ in the energy transport equation (see Eq. (13)) can be scaled as:

$$\rho c_p u_j \frac{\partial T}{\partial x_j} \sim \frac{\rho c_p \vartheta \Delta T}{H} \sim \frac{k\Delta T}{L^2} \times \sqrt{RaPrAR}, \tag{31a}$$

$$\frac{\partial}{\partial x_j}\left(k\frac{\partial T}{\partial x_j}\right) \sim \frac{k\Delta T}{\delta_{th}^2} \sim \frac{k\Delta T}{L^2}\frac{Ra^{1/2} f_1^2(Pr)}{Pr^{1/2} AR^{1/2}}. \tag{31b}$$

Eqs. (31a) and (31b) essentially suggest that the strength of convective transport (Eq. (31a)) increases while the strength of thermal diffusion (Eq. (31b) i.e. conduction) weakens for increasing values of AR when the width of the enclosure L and the temperature difference between the walls ΔT are held constant for a given fluid (i.e. for unaltered values of $k\Delta T/L^2$, Ra and Pr). This trend is consistent with the observation that the thermal transport is primarily conduction-driven for very small values of AR and under this condition convective transport remains very weak (see small aspect ratio cases in Fig. 2a–c). This behaviour can further be substantiated from the distributions of isotherms and stream functions within the enclosure, which are presented in Figs. 3 and 4 for different values of AR at $Ra = 10^4$ and $Ra = 10^6$. For very small values of AR the isotherms remain parallel to the vertical wall indicating conduction-dominated transport whereas the isotherms become curved for higher values of AR as a result of the presence of convection currents. It is also clear from Figs. 3 and 4 that the effects of convection are more pronounced for higher values of AR. Comparison of Figs. 3 and 4 reveals that the effects of convective transport are stronger for higher value of Rayleigh number Ra for a given value of aspect ratio AR because of the higher magnitude of velocity components (see Fig. 2a–c and Eq. (29)). As a result of this strengthening of convective transport, the effects of convection are felt for very small values of aspect ratio AR for higher values

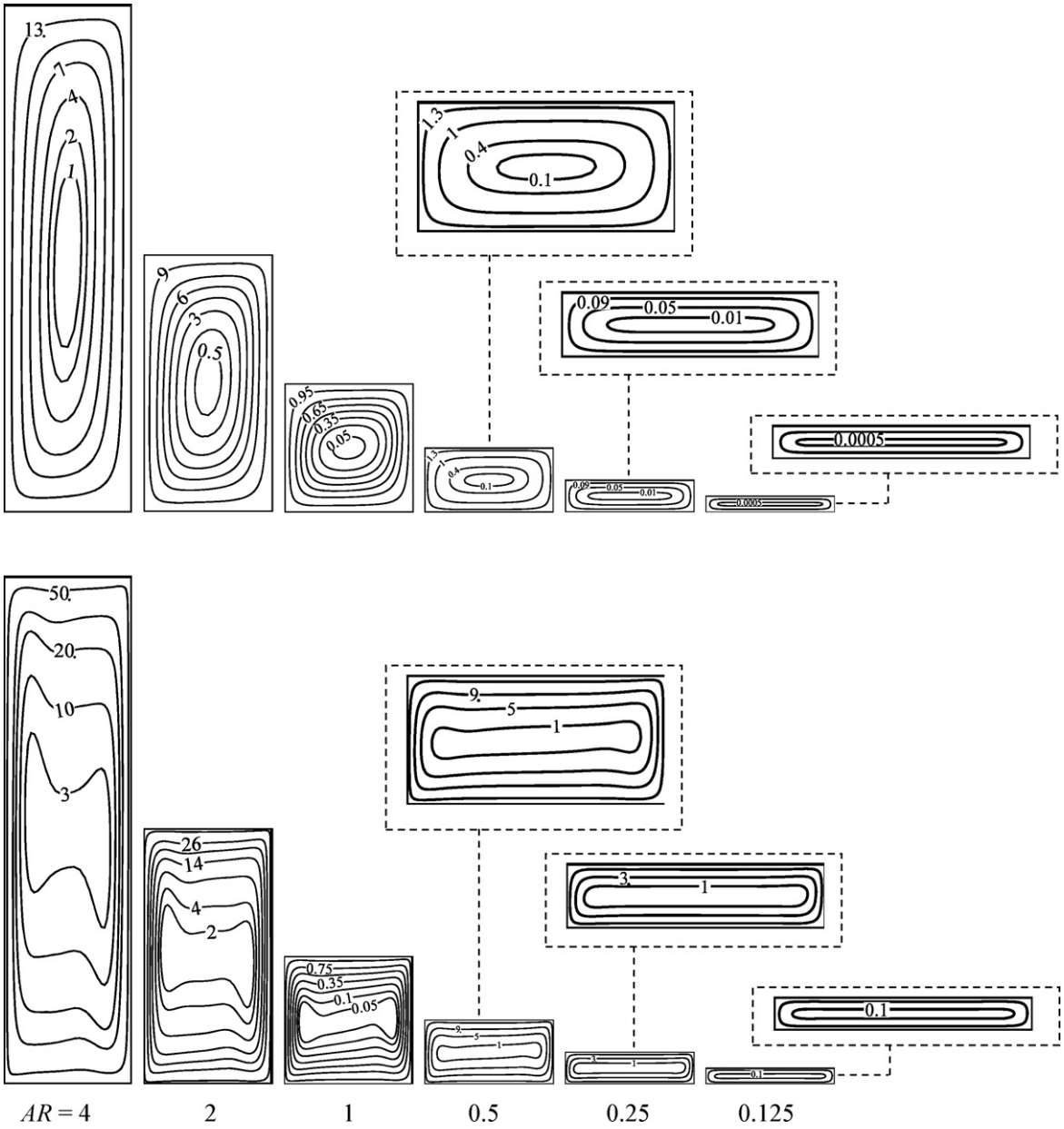

Fig. 4. Contours of stream functions (ψ/α) for convection in Newtonian fluids at $Pr = 7$ for $Ra = 10^4$ (1st row) and $Ra = 10^6$ (2nd row).

of Ra where the thermal transport is primarily conduction-driven for that particular AR for smaller values of Ra (see the $AR = 0.125$ and 0.25 cases in Figs. 3 and 4). The convective energy transfer in the vertical direction within the boundary layer can be scaled as: $\int_0^\delta \rho C_p u_2(\partial T/\partial x_2)\,dx_1 \sim (k\Delta T)Ra^{1/4}(AR)^{3/4}(Pr)^{5/4}$ whereas the vertical thermal transport due to conduction per unit width scales as $\int_0^L -k(\partial T/\partial x_2)\,dx_1 \sim k\Delta T(AR)^{-1}$, which essentially suggests that for Prandtl numbers of the order of unity the convective transport takes precedence over the conduction heat transfer when $Ra^{1/4}AR^{3/4} > AR^{-1}$ or $Ra > AR^{-7}$, which is consistent with the criterion proposed by Bejan et al. [25].

As an increase in aspect ratio AR induces a competition between an increase in advection and a decrease in diffusion strengths, the maximum amount of heat transfer takes place for an optimum value of aspect ratio AR_{max}. It can be inferred from Eqs. (31a) and (31b) that the value of AR_{max} is dependent on Ra for a given value of Pr. Fig. 2a–c and Table 3 indicate that the value of AR_{max} decreases with increasing value of Ra and this behaviour can be seen clearly from the variations of the mean Nusselt number $\overline{Nu}$ with AR for Rayleigh numbers $Ra = 10^4$, 10^5 and 10^6 shown in Fig. 5. It can be seen from Fig. 5 that the correlation for mean Nusselt number $\overline{Nu}$ (see Eq. (21)) proposed by Bejan and Tien [22] satisfactorily captures the variation of $\overline{Nu}$ with AR for $AR < 1$ and the agreement between the prediction of Eq. (21) and the numerical results improves with decreasing value of AR. However, this expression underpredicts the value of $\overline{Nu}$ for the aspect ratios of the order of unity (i.e. $AR \sim 1$). The extent of this underprediction increases with increasing value of Rayleigh number Ra. In addition the expression (Eq. (25)) proposed by Bejan [9] satisfactorily predicts the mean Nusselt number $\overline{Nu}$ with AR for large values of aspect ratio. However, the expression by Bejan [9] overpredicts $\overline{Nu}$ for aspect ratio equal to unity and the extent of this overprediction increases with

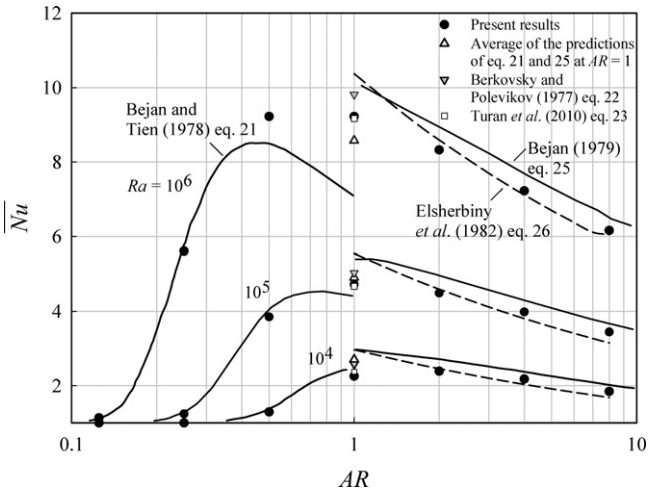

Fig. 5. Variations of mean Nusselt number $\overline{Nu}$ with aspect ratio AR at $Ra = 10^4$, $Ra = 10^5$ and $Ra = 10^6$ for Newtonian fluids ($Pr = 7$).

increasing Ra. The correlation (Eq. (26)) by Elsherbiny et al. [10], although only proposed for $AR > 5$, exhibits satisfactory quantitative agreement with the present simulation data for tall enclosures with $AR \geq 2$. However, the correlation by Elsherbiny et al. [10] (Eq. (26)) also overpredicts the value of $\overline{Nu}$ for square enclosures for all the values of Rayleigh number considered in this study. The arithmetic mean of the predictions of Eqs. (21) and (25) yield a satisfactory agreement with numerical prediction of $\overline{Nu}$ for $AR = 1.0$. The predictions of the correlations proposed by Berkovsky and Polevikov [37] (Eq. (22)) and Turan et al. [27] (Eq. (23)) for square enclosures are also shown in Fig. 5, which indicates that both Eqs. (22) and (23) satisfactorily predict $\overline{Nu}$ for square enclosures.

4.2. Bingham number effects

In order to demonstrate the effects of Bingham number Bn in natural convection of Bingham fluids the distributions of temperature θ and vertical velocity component V with the distance x/L along the horizontal mid-plane (i.e. $y/H = 0.5$) are shown in Fig. 6a–c for different values of Bn and AR at a nominal Rayleigh number $Ra = 10^6$ and $Pr = 7$. The same qualitative behaviour is observed for other values of Ra and are therefore not shown here for the sake of conciseness. The use of the exponential form of the Bingham model (due to Papanastasiou [31]) was found to give virtually identical results. The variation in Nusselt number between the regularisations for nominally identical conditions was typical less than 0.1% and only at very large Bingham numbers, when the Nusselt number approaches unity, were small differences apparent (still less than 3% in $\overline{Nu}$). These differences are on the same order as the differences between results in the bi-viscosity model for different values of the yield viscosity parameter and are, for all practical purposes, unimportant for the discussion which follows.

Comparing the results in Fig. 6a–c it is evident that the value of the aspect ratio AR_{max} at which the maximum $\overline{Nu}$ value is obtained increases with increasing Bn and the temperature gradient in the vicinity of the vertical walls decreases with increasing value of Bn for a given value of AR. Moreover, the non-linearity of the temperature θ variation decreases with increasing value of Bn for a given set of values of nominal Rayleigh number Ra and aspect ratio AR. This decrease essentially suggests that the effects of convection weaken with increasing value of Bingham number Bn. Further evidence of this effect can be seen in the variations of the vertical velocity V with normalised distance x/L along the horizontal mid-plane (r.h.s. of Fig. 6), which confirm that the strength of convection weakens with increasing value of Bingham number Bn. The relative strength of viscous forces in comparison to buoyancy force increases with increasing Bn for a given value of nominal Rayleigh number Ra. As a result of this strengthening of viscous forces, the fluid flow in the enclosure eventually becomes too weak to influence the thermal transport due to convective heat transfer for $Bn > Bn_{max}$ and under this condition heat transfer takes place predominantly due to thermal conduction, which is reflected by a unity value of mean Nusselt number (i.e. $\overline{Nu} = 1$). For a given value of Ra the effects of convection remain important for $Bn < Bn_{max}$ and thermal diffusion (conduction) remains the predominant mode of heat transfer for $Bn \geq Bn_{max}$. It is worth noting that a flow of diminishing strength with increasing Bingham number will always be obtained in the context of bi-viscosity [30] and Papanastasiou [31] regularisations of the Bingham model and complete stoppage of fluid flow will only be obtained if a ideal Bingham model (i.e. Eqs. (1) and (2)) is implemented. However, identifying the point accurately at which the fluid flow ceases to exist is not of major significance in the context of the present study as this article primarily deals with heat transfer rate behaviour in Bingham fluids and the fluid flow becomes weak enough to influence the thermal transport even before the flow ceases to exist in Bingham fluids. Thus $Bn \geq Bn_{max}$ is a sufficient condition for $\overline{Nu} = 1$ but it is not necessary condition for the fluid flow to cease and it is possible to have fluid flow for $Bn \geq Bn_{max}$ but this flow will be too weak to impart any perceptible influence on thermal transport.

The aforementioned behaviour can be seen from the contours of temperature and stream function for different values of AR and Bn for $Ra = 10^6$ in Figs. 7 and 8 respectively, which show that the weakening of convection with increasing Bn is more readily felt for enclosures with small aspect ratio. For large values of Bingham number (i.e. $Bn \geq Bn_{max}$) the isotherms become parallel to the vertical walls indicating pure conduction heat transfer. The "unyielded" zones (zones of fluid where $|\tau| \leq \tau_y$ according to the criterion used by Mitsoulis [29]) are also shown in Fig. 8. It is worth noting that these zones are not really "unyielded" in the true sense as pointed out by Mitsoulis and Zisis [39]. In the present study a bi-viscosity approximation is used to model the Bingham fluid flow so flow will always be present within these essentially very high viscosity regions, which can alternatively be viewed as regions of extremely slowly moving fluid and these regions were termed "apparently unyielded regions (AUR)" in Ref. [39]. It is important to stress that these small islands of AUR are dependent on the choice of μ_{yield} (shown in Fig. 8 for $\mu_{yield} = 10^4\,\mu$) while the mean Nusselt number, the stream function and the zones of AUR at the corners of the enclosure remain independent of μ_{yield} for $\mu_{yield} \geq 10^4\,\mu$. For a given value of τ_y the zones with very low shear rate, which satisfy $|\tau| \leq \tau_y$ shrink with an increase in μ_{yield}. As the AUR zones are dependent on the choice of μ_{yield}, in-depth discussion of their significance is not considered appropriate for the objectives of this paper.

The heat and fluid flow characteristics observed in Figs. 6–8 can be explained using the scaling arguments for the aspect ratios for which convective transport plays a non-negligible role. The balance of inertial and viscous forces in the momentum transport equation in the boundary layer adjacent to the vertical side walls yields:

$$\rho\frac{\vartheta^2}{H} \sim \left(\tau_y + \mu\frac{\vartheta}{\delta}\right)\frac{1}{\delta}. \tag{32}$$

Based on Eq. (32) one obtains a scaling estimate of the hydrodynamic boundary layer thickness δ:

$$\delta \sim \frac{1}{2}\frac{\tau_y H}{\rho\vartheta^2} + \frac{1}{2}\frac{H}{\rho\vartheta^2}\sqrt{\tau_y{}^2 + 4\rho\frac{\vartheta^3}{H}\mu}. \tag{33}$$

Using Eq. (28) and the definitions of Bn and Ra one obtains the following estimate of the hydrodynamic boundary layer thickness

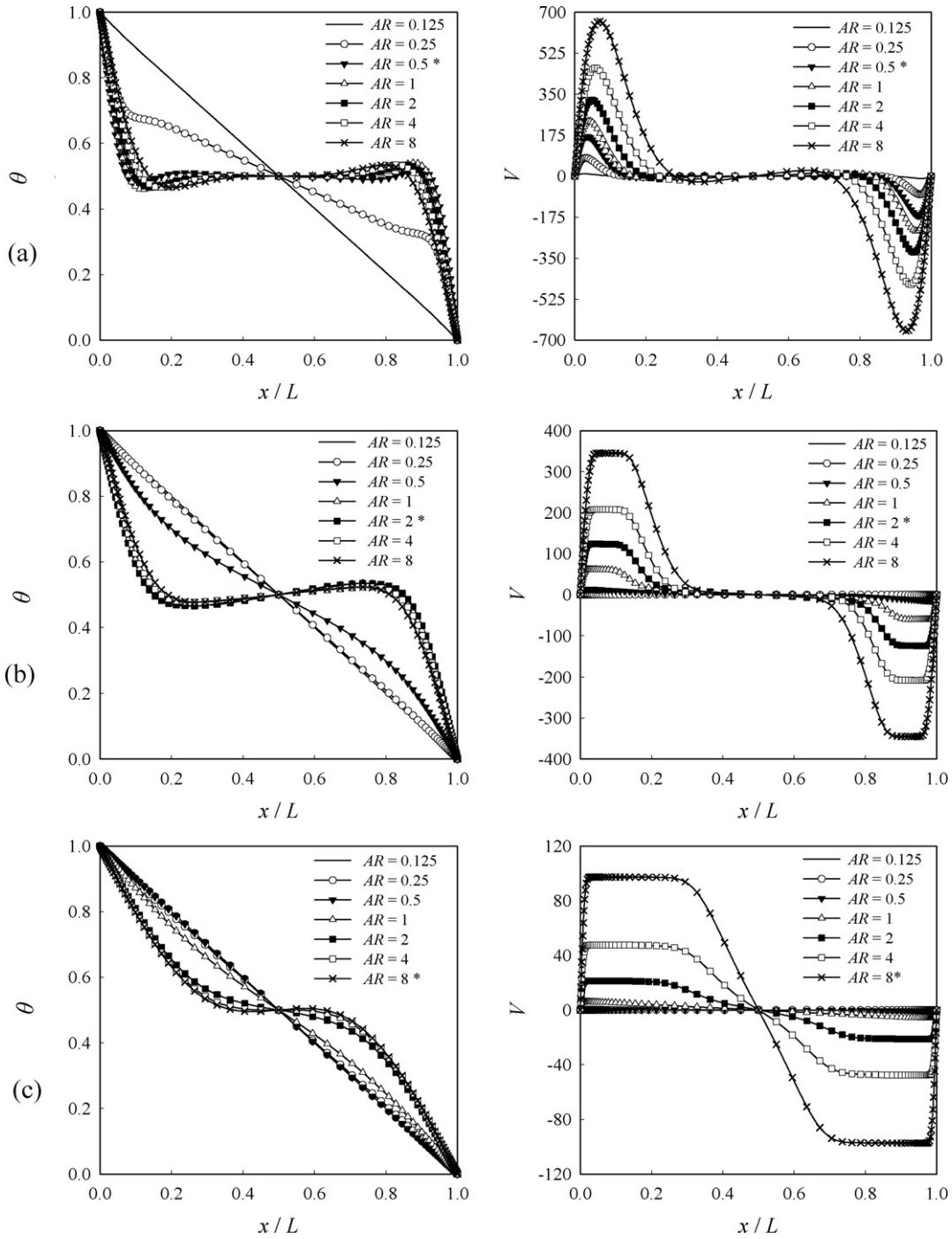

Fig. 6. Variations of temperature θ and vertical velocity component V along the horizontal mid-plane (i.e. $y/H = 0.5$) for Bingham fluids case at $Ra = 10^6$ and $Pr = 7$: (a) $Bn = 0$, (b) $Bn = 3$ and (c) $Bn = 10$ (asterisk (*) highlights AR in which the maximum mean Nusselt number $\overline{Nu}$ occurs).

δ, when ϑ is non-negligible.

$$\delta \sim \frac{L}{\sqrt{Ra/Pr}} \left[\frac{Bn}{2} + \frac{1}{2}\sqrt{Bn^2 + 4AR^{1/2}\left(\frac{Ra}{Pr}\right)^{1/2}} \right]. \tag{34}$$

This scaling gives rise to the following expression for the thermal boundary layer thickness δ_{th}:

$$\delta_{th} \sim \min\left[L, \frac{L.Pr^{1/2}}{f_2(Bn, Pr)Ra^{1/2}} \left[\frac{Bn}{2} + \frac{1}{2}\sqrt{Bn^2 + 4\sqrt{AR}\left(\frac{Ra}{Pr}\right)^{1/2}} \right] \right]. \tag{35a}$$

where $f_2(Bn, Pr)$ is a positive-definite function (i.e. $f_2(Bn, Pr) > 0$) such that it increases with increasing value of Pr and also may have some Bingham number Bn dependence. Using the scaling given in Eq. (35a) it is possible to estimate the Bingham number Bn_{max} below which convection starts to play an important role (i.e. $\overline{Nu} > 1$). In this regard it is worth noting that $\overline{Nu} = 1$ does not indicate that the whole flow field is unyielded (some weak flow, albeit insufficient to affect the thermal transport, may still be occurring). For $\overline{Nu} = 1$ the thermal boundary layer thickness δ_{th} becomes of the same order as the enclosure width L. (i.e. $\delta_{th} \sim L$), which gives rise to following

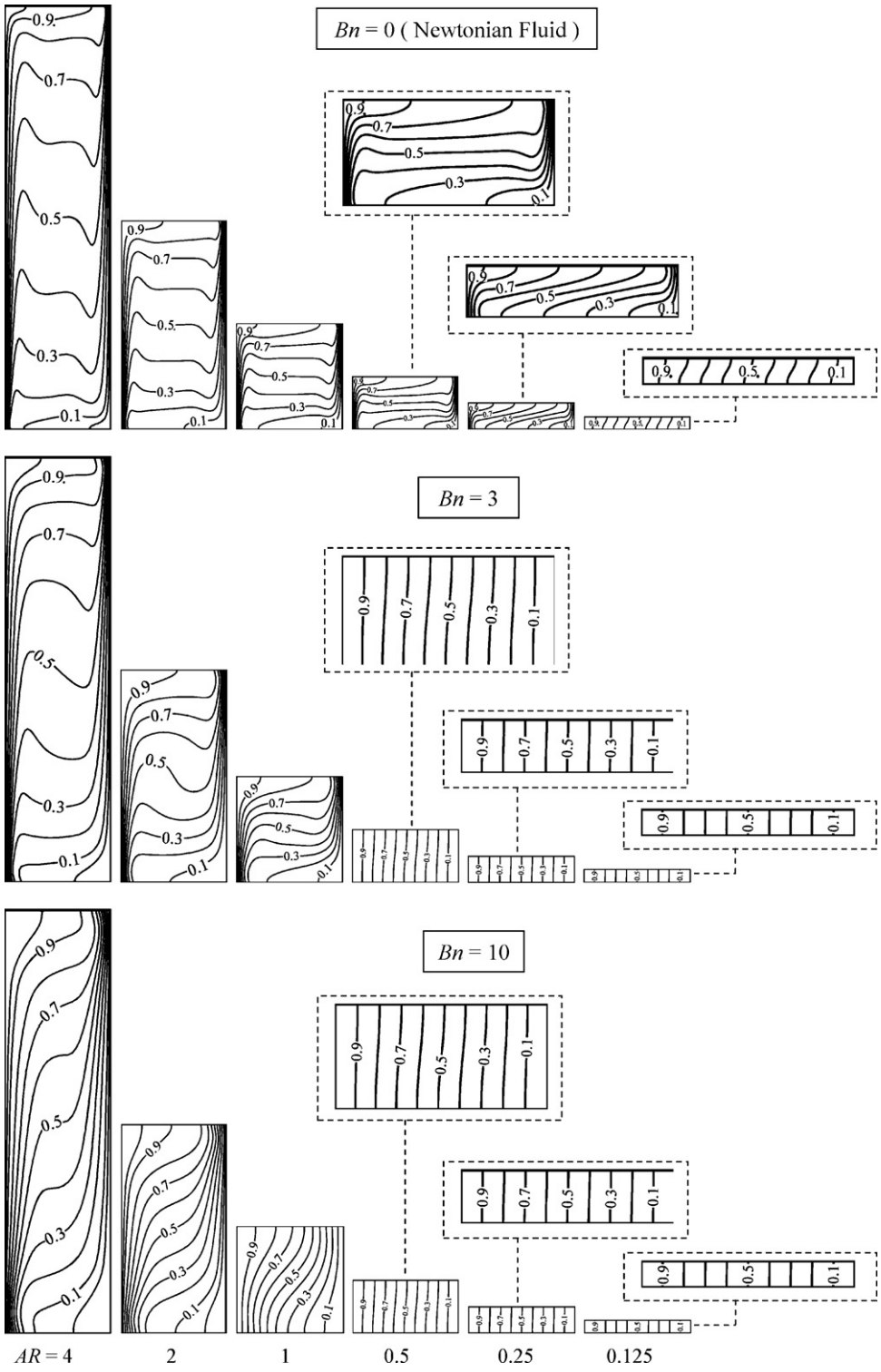

Fig. 7. Contours of temperature θ for convection in Bingham fluids at $Pr = 7$ for $Ra = 10^6$.

estimate for $Bn_{\max}$ using Eq. (35a):

$$Bn_{\max} \sim \sqrt{\frac{Ra}{Pr}} f(Bn_{\max}, Pr) - \frac{\sqrt{AR}}{f_2(Bn_{\max}, Pr)}. \tag{35b}$$

The critical Bingham number Bn_{crit} where the buoyancy force is just sufficient to overcome the yield stress leads to unyielded fluid throughout the domain yet $\overline{Nu}$ remains equal to unity. The equilibrium of buoyancy and yield stress effects gives rise to the following condition:

$$\rho g \beta \Delta T \sim \frac{\tau_y}{\delta} \sim \frac{\tau_y}{L f_2(Bn_{crit}, Pr)}. \tag{35c}$$

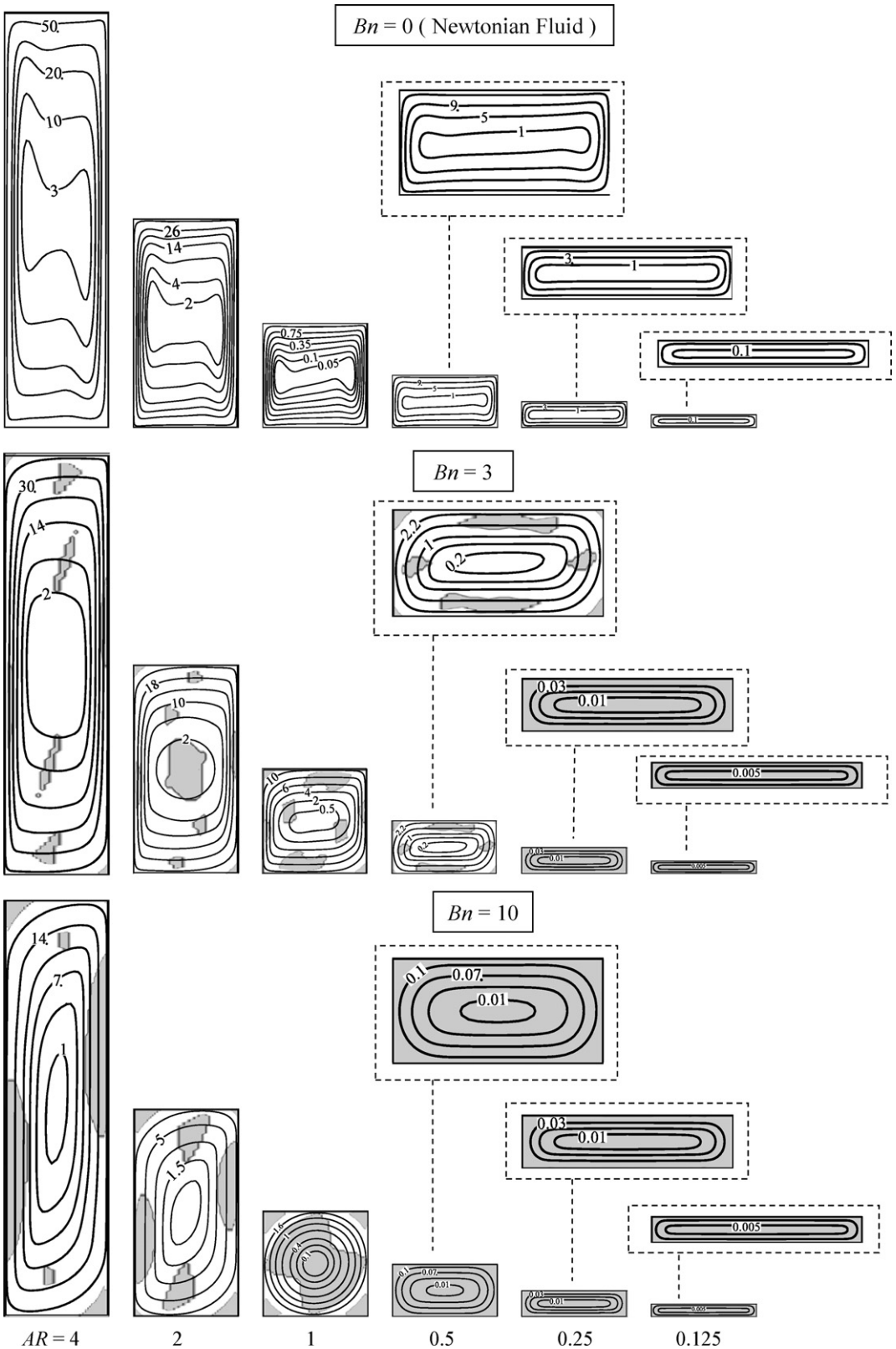

Fig. 8. Contours of stream functions (ψ/α) and unyielded zones (shown in grey) for convection in Bingham fluids at $Pr = 7$ for $Ra = 10^6$.

The above relation can further be rewritten as:

$$Bn_{crit} \sim \sqrt{\frac{Ra}{Pr}} f_2(Bn_{crit}, Pr) \tag{35d}$$

Eq. (35d) is consistent with the recent analytical results of Vikhanisky [40] for the onset of natural convection in rectangular enclosures. According to Vikhanisky [40] Bn_{crit} is given by:

$$Bn_{crit} = \frac{0.25\sqrt{Ra/Pr}}{1 + 0.96/AR + 4/AR^2}. \tag{35e}$$

However, it is worth reiterating that $Bn \geq Bn_{crit}$ ensures that $\overline{Nu}$ remains equal to unity but it does not imply that $\overline{Nu} > 1$ when Bn is smaller than Bn_{crit}. The mean Nusselt number $\overline{Nu}$ only attains a value greater than unity when Bn is smaller than $Bn_{\max}$. Comparing Eqs. (35c) and (35d) it is clear that $Bn_{\max}$ is smaller than Bn_{crit} and the difference between Bn_{crit} and $Bn_{\max}$ is likely to increase with increasing aspect ratio AR.

Eq. (35a) can be used to estimate the thermal diffusion terms in the energy transport equation:

$$\frac{\partial}{\partial x_j}\left(k\frac{\partial T}{\partial x_j}\right) \sim \frac{k\Delta T}{\delta_{th}^2} \sim \frac{k\Delta T}{L^2} Max\left[1, \frac{(Ra/Pr)^{1/2}[f_2(Bn, Pr)]^2}{\sqrt{AR}[0.5\, BnPr^{1/4}/(Ra^{1/4}AR^{1/4}) + 0.5\sqrt{[BnPr^{1/4}/(Ra^{1/4}AR^{1/4})]^2 + 4}]^2}\right]. \tag{36}$$

Comparing Eq. (36) with (31b) reveals that the effects of thermal diffusion weaken with increasing Bingham number Bn when Ra, Pr and AR are held constant: essentially indicating that the thermal diffusion strength for given values of nominal Rayleigh number and Prandtl number weakens with increasing values of Bn^*, which is defined as:

$$Bn^* = \frac{Bn}{(RaAR/Pr)^{1/4}}. \tag{37}$$

Eq. (37) suggests that for a given set of values of Ra and Pr, a decrease in AR reduces the strength of thermal diffusion in comparison to the corresponding Newtonian situation.

The relative strengths of buoyancy forces to viscous forces can be characterised by the Grashof number Gr (=Ra/Pr) but in Bingham fluids it can be more appropriate to use an effective viscosity μ_{eff} (see detailed discussion in Turan et al. [27]):

$$\mu_{eff} = \mu + \frac{\tau_y}{\dot{\gamma}}. \tag{38}$$

The strain rate can be scaled as $\dot{\gamma} \sim \vartheta/\delta$, which yields the following estimation of μ_{eff}:

$$\mu_{eff} \sim \mu\left[1 + Bn^*\left[\frac{Bn^*}{2} + \frac{1}{2}\sqrt{Bn^{*2} + 4}\right]\right]. \tag{39}$$

Based on Eq. (39) an effective Grashof number Gr_{eff} can be defined as:

$$Gr_{eff} = \frac{\rho^2 g\beta\Delta T L^3}{\mu_{eff}^2} \sim Gr\left[1 + Bn^*\left[\frac{Bn^*}{2} + \frac{1}{2}\sqrt{Bn^{*2} + 4}\right]\right]^{-2}. \tag{40}$$

Table 4
Variations of $Bn_{\max}$ with aspect ratio (AR) in the case of Bingham fluids for $Ra = 10^4 - 10^6$ and $Pr = 7$.

AR	$Ra = 10^4$	$Ra = 10^5$	$Ra = 10^6$
0.125	–	–	0.19
0.25	–	0.26	1.10
0.5	0.28	1.18	3.99
1.0	1.05	3.53	11.6
2	1.49	4.99	16.5
4	1.90	6.00	19.9
8	1.92	6.97	21.8

Thus a decrease (an increase) in AR gives rise to an increase (decrease) in Bn^* for a given set of values of Ra, Pr and Bn, which in turn acts to reduce (increase) the effective Grashof number Gr_{eff} in comparison to the Grashof number (i.e. $Gr = Ra/Pr$) for the Newtonian case. The strength of viscous effects relative to buoyancy forces increase (decrease) with decreasing (increasing) aspect ratio AR, which is consistent with the decreasing magnitudes of vertical velocity component V and stream function ψ/α with decreasing AR in Figs. 6a–c and 8 respectively (when the Ra, Pr and Bn are held constant). Moreover, for a given set of values of Ra, Pr and AR, an increase in Bn leads to an increase in Bn^*, which in turn reduces the effective Grashof number Gr_{eff} in comparison to the Grashof number (i.e. $Gr = Ra/Pr$) for the Newtonian case. The decreasing magnitudes of V and ψ/α with increasing Bn in Figs. 6a–c and 8 respectively (again when Ra, Pr and AR are held constant) indicates that the effects of buoyancy-driven flow weaken with increasing value of Bingham number Bn in agreement with this argument.

Eq. (35a) can be used to estimate the mean Nusselt number $\overline{Nu}$ in the boundary-layer regime [22] for natural convection of Bingham fluids in rectangular enclosures in the following way:

$$q_f \sim h\Delta T \sim k\frac{\Delta T}{\delta_{th}} \quad \text{or} \quad \overline{Nu} \sim \frac{hL}{k} \sim \frac{L}{\delta_{th}}. \tag{41}$$

Using Eqs. (35a) and (41) one obtains the following scaling estimate of $\overline{Nu}$:

$$\overline{Nu} \sim Max\left[1.0, \frac{Ra^{1/2}/Pr^{1/2}}{\left[Bn/2 + 1/2\sqrt{Bn^2 + 4\sqrt{AR}\left(Ra/Pr\right)^{1/2}}\right]} f_2(Pr, Bn)\right], \tag{42a}$$

which can alternatively be written as:

$$\overline{Nu} \sim Max\left[1.0, \frac{\overline{Nu}_{Bn=0}}{\left[Bn^*/2 + 1/2\sqrt{Bn^{*2} + 4}\right]} f_3(Pr, Bn)\right], \tag{42b}$$

where $f_3(\mathrm{Pr}, Bn) = f_2(\mathrm{Pr}, Bn)/f_1(\mathrm{Pr})$ and $\overline{Nu}_{Bn=0}$ is the mean Nusselt number for Newtonian fluids for the same nominal values of Ra and Pr, which can be obtained by setting $Bn = 0$ in Eq. (42a). Doing so yields $\overline{Nu} \sim Ra^{0.25} f_2(Pr, 0)/Pr^{0.25}$ for Newtonian fluids in square enclosures and is in good agreement with the correlations given by Eqs. (22) and (23), which suggest that the mean Nusselt number $\overline{Nu}$ is directly proportional to $Ra^{0.29}$. Given the simplicity of the scaling analysis, it is not unexpected that a small quantitative difference between the value of exponent of Ra between the scaling prediction and the correlation function exists (0.25 cf. 0.29). However, the qualitative trends are accurately captured by the scaling relations. Moreover, it has been proposed by Gill [6] that $\overline{Nu}$ asymptotically approaches to $\overline{Nu} = 0.364[Ra/(PrAR)]^{1/4}$ for large values of AR, which is in remarkable agreement with the present scaling estimate: in this limit Eq. (42a) reduces to $\overline{Nu} \sim [Ra/(PrAR)]^{1/4}$ for Newtonian fluids.

In the parallel-flow regime (i.e. $Ra\, AR^3 \to 0$) the vertical velocity component at the core of the enclosure disappears and the fluid flow in the enclosure consists of two counter-flowing horizontal streams and the temperature gradient in the horizontal direction $K = \partial T/\partial x_1 \sim \Delta T/L$ remains constant. It is worth noting

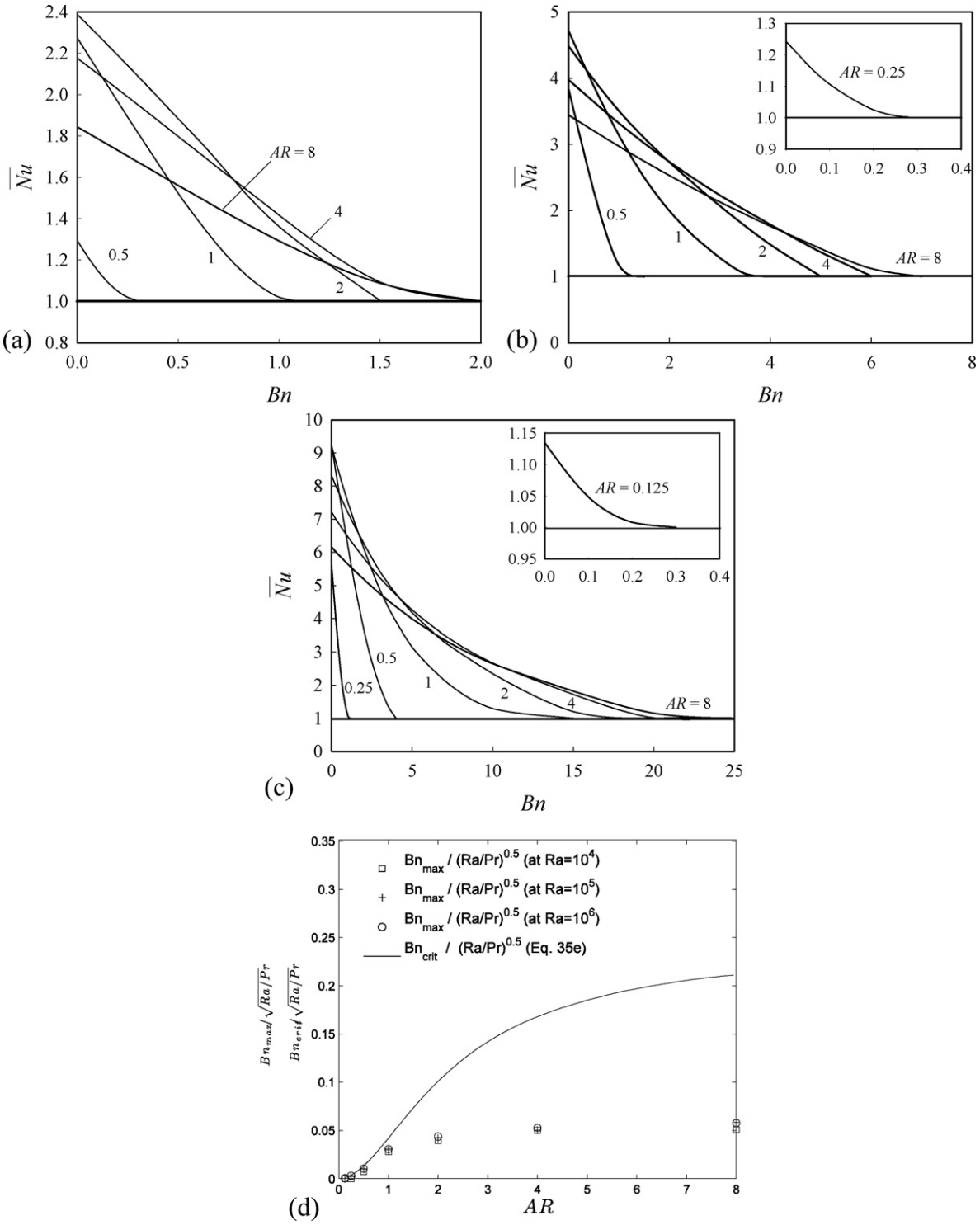

Fig. 9. Variations of mean Nusselt number $\overline{Nu}$ with Bingham number Bn for different values of aspect ratio at $Pr = 7$: (a) $Ra = 10^4$, (b) $Ra = 10^5$ and (c) $Ra = 10^6$. (d) Variations of $Bn_{\max}/\sqrt{Ra/Pr}$ with AR for $Ra = 10^4$, 10^5 and 10^6 at $Pr = 7$. The variations of $Bn_{crit}/\sqrt{Ra/Pr}$ with AR for $Ra = 10^4$, 10^5 and 10^6 at $Pr = 7$ according to Eq. (35e).

that $RaAR^3 \to 0$ does not imply the effects of convection are likely to be weak because one may obtain the parallel-flow regime even in the presence of non-negligible values of Rayleigh number Ra for very small values of aspect ratio. This issue has been discussed in detail by Bejan and Tien [22]. In the parallel-flow regime the equilibrium of vorticity generation/destruction by buoyancy and the molecular diffusion of vorticity at the middle of the domain yields:

$$\rho g\beta K \sim -\frac{\partial^2 \tau_{12}}{\partial x_2^2} \quad \text{or} \quad \rho g\beta \frac{\Delta T}{L} \sim \frac{\partial}{\partial x_2^2}\left[\mu \frac{\partial u_1}{\partial x_2} + \tau_y\right] \quad \text{or} \quad \rho g\beta \frac{\Delta T}{L} \sim \frac{\mu u_c}{F^3 H^3} + \frac{\tau_y}{(FH)^2}, \tag{43a}$$

which leads to the following scaling for the horizontal velocity component at the core:

$$u_c \sim F^3\left(\frac{\rho g \beta K H^3}{\mu}\right) - F\left(\frac{\tau_y H}{\mu}\right) \quad \text{or} \quad u_c \sim F^3 Ra\, AR^3\left(\frac{\alpha}{L}\right) \times \left[1 - F^{-2} Bn\left(\frac{Pr}{Ra}\right)^{1/2}/AR^2\right], \tag{43b}$$

where the hydrodynamic boundary layer thickness on horizontal surfaces is scaled as: $\delta \sim F\,H$ with F being an appropriate fraction (i.e. $0 < F < 1$). Using the balance of convective and diffusive terms of the energy transport equation gives:

$$\rho c_p u_1 \frac{\partial T}{\partial x_1} \sim k \frac{\partial^2 T}{\partial x_2^2} \quad \text{or} \quad \rho c_p u_c \frac{\Delta T}{L} \sim k \frac{\Delta T_1}{F^2 H^2} f_4(Pr, Bn)^2, \tag{44a}$$

which yields:

$$u_c K \sim \frac{k}{L^2}\Delta T F^3 Ra AR^3[1 - F^{-2} Bn^{**}] \sim \frac{k f_4(Pr, Bn)^2}{F^2 H^2}\Delta T_1 \text{ or } \Delta T_1 \sim \frac{Ra F^5 AR^5 \Delta T[1 - F^{-2} Bn^{**}]}{f_4(Pr, Bn)^2}, \tag{44b}$$

where ΔT_1 is the characteristic temperature difference between the horizontal adiabatic walls and the thermal boundary layer thickness adjacent to the horizontal walls is scaled as: $\delta_{th} \sim FH/f_4(Bn, \mathrm{Pr})$. In Eq. (44b) the quantity Bn^{**} is defined as:

$$Bn^{**} = \frac{Bn}{(Ra/Pr)^{1/2} AR^2}. \tag{44c}$$

For Newtonian fluids (i.e. $Bn = 0$) ΔT_1 scales as $\Delta T_1 \sim Ra F^5 AR^5 \Delta T / f_4(\mathrm{Pr})$, which is consistent with the analytical results of Cormack et al. [20] (i.e. $\Delta T_1 = Ra\, AR^5 (T_H - T_C)/720$). Using Eqs. (43b) and (44b) the mean Nusselt number $\overline{Nu}$ can be estimated by the following integral at the middle of the domain:

$$\overline{Nu} = \overline{Nu}_1 + \overline{Nu}_2, \tag{45a}$$

where

$$\overline{Nu}_1 = \frac{L}{Hk\Delta T}\int_0^H \rho c_p u_1 T\, dx_2 \quad \text{and} \quad \overline{Nu}_2 = -\frac{L}{Hk\Delta T}\int_0^H k\frac{\partial T}{\partial x_1}\, dx_2. \tag{45b}$$

Using Eqs. (43b) and (44b) $\overline{Nu}_1$ can be scaled as:

$$\overline{Nu}_1 = \frac{L}{Hk\Delta T}\int_0^H \rho c_p u_1 T\, dx_2 \sim \frac{L \rho c_p u_c \Delta T_1 H}{Hk\Delta T} \sim \frac{Ra^2 F^8 AR^8 [1 - F^{-2} Bn^{**}]^2}{f_4(Bn, Pr)^2}, \tag{46a}$$

whereas $\overline{Nu}_2$ can be scaled as:

$$\overline{Nu}_2 = -\frac{L}{Hk\Delta T}\int_0^H k\frac{\partial T}{\partial x_1}\, dx_2 = \frac{H\Delta T L k}{H\Delta T L k} = 1. \tag{46b}$$

Thus in the parallel-flow regime (i.e. $Ra AR^3 \to 0$) the mean Nusselt number $\overline{Nu}$ can be given as:

$$\overline{Nu} = 1 + \frac{a Ra^2 F^8 AR^8 (1 - F^{-2} Bn^{**})^2}{f_4(Bn, Pr)^2}, \tag{47a}$$

where a is an appropriate constant. Setting $Bn = 0$ suggests that $\overline{Nu} = 1 + a F^8 Ra^2 AR^8 / f_4^2$ for Newtonian fluids in the $Ra AR^3 \to 0$ limit which is indeed found to be in good agreement with the asymptotic result of Cormack et al. [20] (i.e. $\overline{Nu} = 1 + Ra^2 AR^8/362880$): indicating $F \sim 1/5$ for $a = 1$ and $f_4 \approx 1.0$. Using the $\overline{Nu}$ scaling of Newtonian fluids, Eq. (47a) can be rewritten in the following manner:

$$\frac{\overline{Nu} - 1}{(\overline{Nu})_{Bn=0} - 1} \sim (1 - F^{-2} Bn^{**})^2 \frac{f_4(Pr)^2}{f_4(Bn, Pr)^2} \quad \text{when } (\overline{Nu})_{Bn=0} > 1, \tag{47b}$$

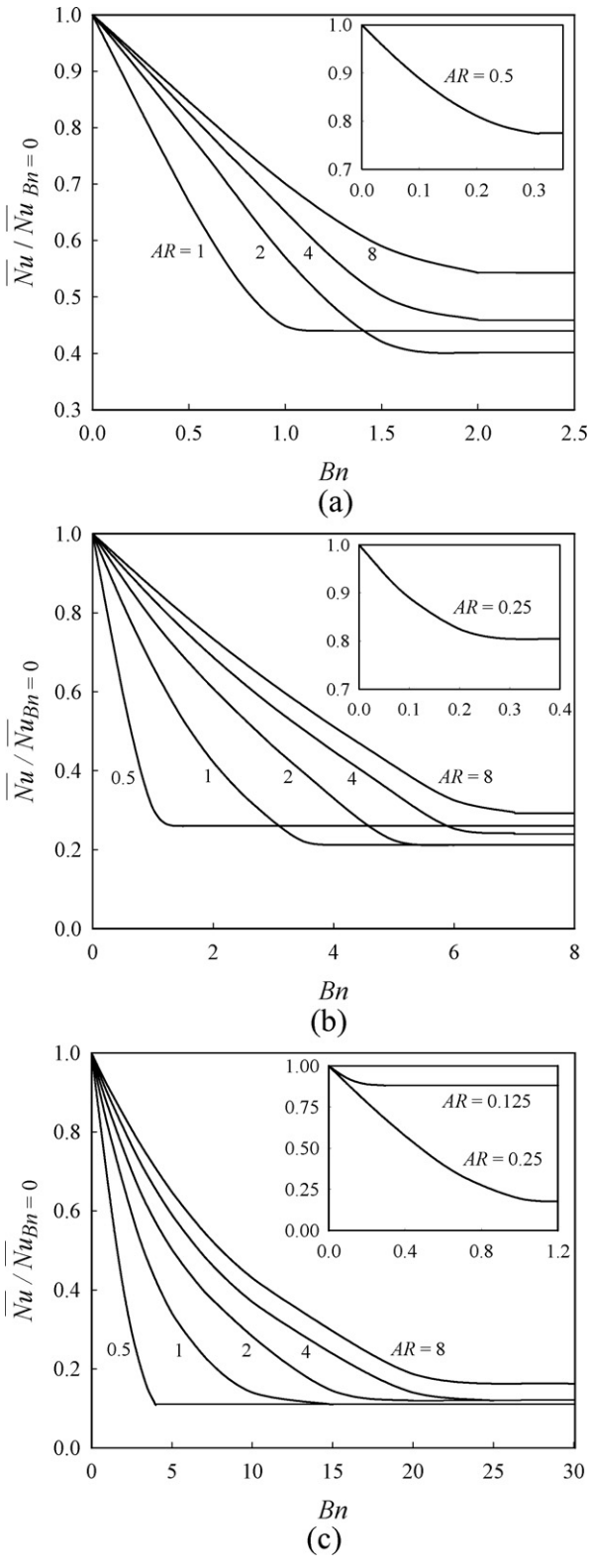

Fig. 10. Variations of $\overline{Nu}/\overline{Nu}_{Bn=0}$ with Bingham number Bn for different values of aspect ratio at $Pr = 7$: (a) $Ra = 10^4$, (b) $Ra = 10^5$ and (c) $Ra = 10^6$.

$$\overline{Nu} = 1 \quad \text{when } (\overline{Nu})_{Bn=0} = 1 \tag{47c}$$

The scaling relations given by Eqs. (42) and (47) provide useful insight into the anticipated behaviour of $\overline{Nu}$ in response to variations of Ra, Pr and Bn. The above analysis suggests that $\overline{Nu}$ is expected to decrease with increasing Bn for a given value of

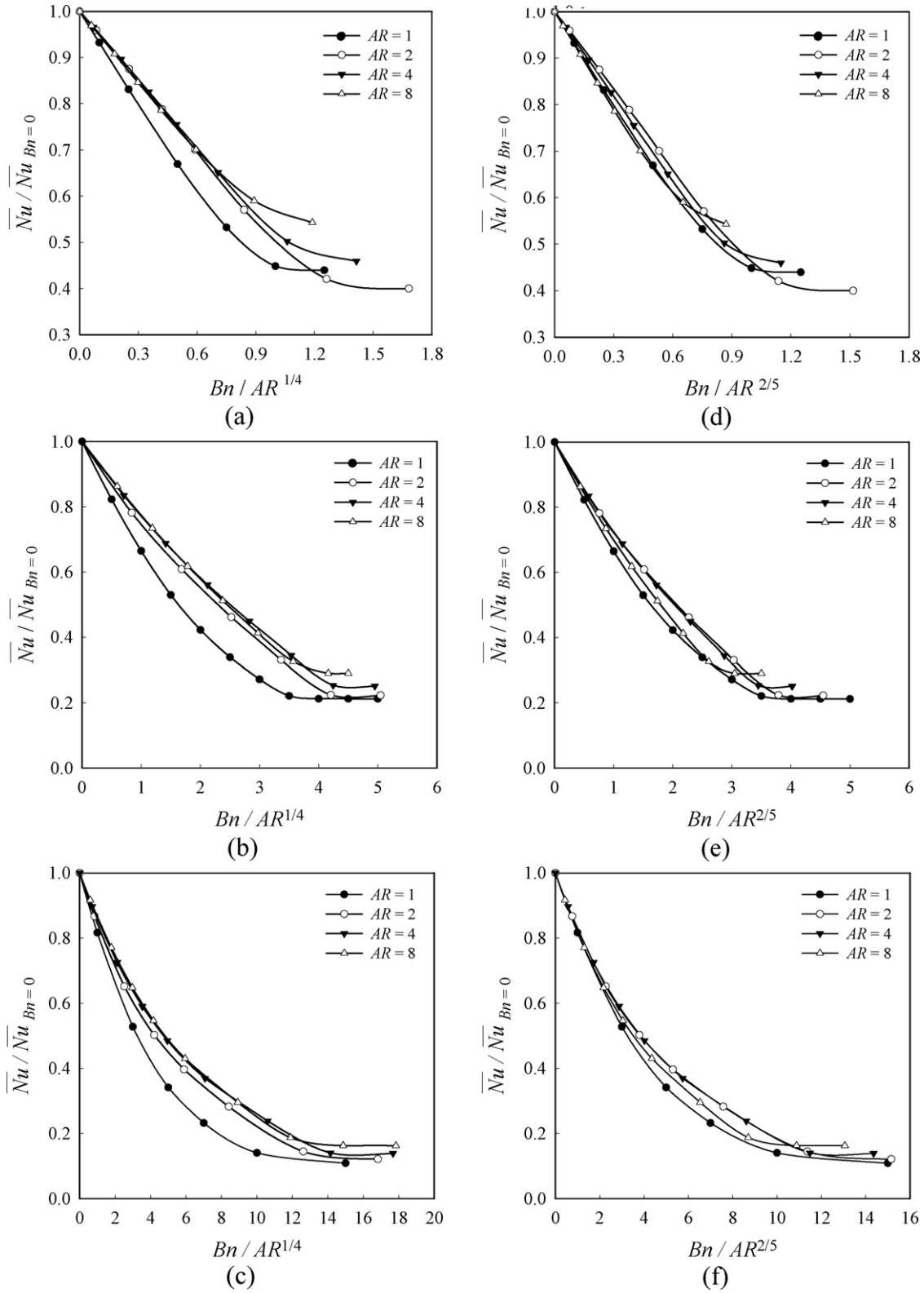

Fig. 11. Variations of $\overline{Nu}/\overline{Nu}_{Bn=0}$ with $Bn/AR^{1/4}$ for $AR \geq 1$ cases at $Pr = 7$: (a) $Ra = 10^4$, (b) $Ra = 10^5$ and (c) $Ra = 10^6$. Variation of $\overline{Nu}/\overline{Nu}_{Bn=0}$ with $Bn/AR^{2/5}$ for $AR \geq 1$ cases at $Pr = 7$: (d) $Ra = 10^4$, (e) $Ra = 10^5$ and (f) $Ra = 10^6$.

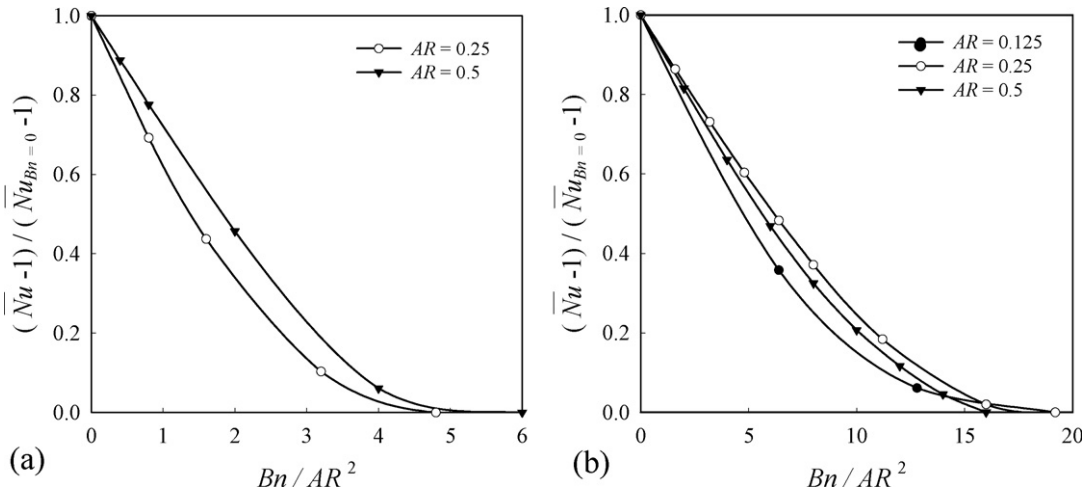

Fig. 12. Variations of $(\overline{Nu}-1)/(\overline{Nu}_{Bn=0}-1)$ with Bn/AR^2 for $AR<1$ cases at $Pr=7$: (a) $Ra=10^5$ and (b) $Ra=10^6$.

Ra whereas $\overline{Nu}$ increases with increasing Ra for a given value of Bn.

The variations of $\overline{Nu}$ with Bn for $Ra=10^4$, 10^5 and 10^6 are shown in Fig. 9a–c respectively for $Pr=7.0$, which demonstrate that $\overline{Nu}$ decreases with increasing value of Bn for all the values of aspect ratio AR studied. It has been discussed earlier in the context of Eq. (40) that viscous effects become increasingly strong in comparison to buoyancy effects for increasing Bn. As a result of this augmented viscous effect, fluid flow eventually ceases to influence the heat transfer within the enclosure once Bn attains a threshold value $Bn_{\max}$. The effects of convection are important for $Bn<Bn_{\max}$ and for $Bn\geq Bn_{\max}$ the heat transfer takes place predominantly due to conduction. That heat transfer is predominantly due to conduction is reflected in the unity value of $\overline{Nu}$ for $Bn\geq Bn_{\max}$. Moreover, comparing Fig. 9a–c it can be seen that $\overline{Nu}$ increases with increasing Ra for a given set of values of Pr, Bn and AR. The variation of $\overline{Nu}$ in response to Ra and Bn for different aspect ratios are found to be consistent with previous studies in square enclosures by Vola et al. [26] and Turan et al. [27]. As convection strengthens with increasing Ra for a given set of values of Pr and AR, the effects of buoyancy-driven flow can counter viscous effects up to a larger value of Bingham number, which is reflected in the increase in $Bn_{\max}$ with increasing Ra. The values of $Bn_{\max}$ are estimated here by carrying out simulations and identifying the Bingham number at which $\overline{Nu}$ obtains a value of 1.01 and the values of $Bn_{\max}$ for the values of Ra and AR are listed in Table 4. Although this definition of $Bn_{\max}$ appears to be somewhat arbitrary, in this configuration convection is always present and so $\overline{Nu}=1$ is an asymptotic limit. In addition uncertainties due to the level of mesh refinement and the choice of the regularisation (and, indeed, the exact value of μ_{yield}) are largest close to this situation and preclude a more stringent criterion. Nevertheless identifying $Bn_{\max}$ with $\overline{Nu}=1.005$ alters the values by less than 5%. The variation of $Bn_{\max}/\sqrt{Ra/Pr}$ with AR is shown in Fig. 9d for $Ra=10^4$, 10^5 and 10^6, which demonstrates that the value of $Bn_{\max}$ increases with increasing AR for all values of Ra considered here. Moreover, it can be seen from Fig. 9d that the variations of $Bn_{\max}/\sqrt{Ra/Pr}$ with AR for different values of Ra remain close but do not collapse. It is worth noting that Eq. (35b) provides just a scaling estimate for $Bn_{\max}$ but it is not sufficient to predict the variation of $Bn_{\max}/\sqrt{Ra/Pr}$ with AR. However, a lack of collapse of $Bn_{\max}/\sqrt{Ra/Pr}$ is expected according to Eq. (35b) due to the involvement of the term $f_2(Bn_{\max}, Pr)$. The variation of $Bn_{crit}/\sqrt{Ra/Pr}$ with AR according to Eq. (35e) is also shown on Fig. 9d, which shows that Bn_{crit} remains greater than $Bn_{\max}$ for all values of Ra and this difference increases with increasing AR which is also consistent with the expectations from the scaling estimates given by Eqs. (35c) and (35d).

It can be noticed from Fig. 9a–c that the variation of $\overline{Nu}$ with Bn does not exhibit monotonic behaviour in terms of aspect ratio AR. This behaviour originates due to non-monotonic AR dependence of $\overline{Nu}$ in Newtonian fluids (i.e. $\overline{Nu}$ at $Bn=0$). This effect is demonstrated in Fig. 10a–c where the variations of $\overline{Nu}/\overline{Nu}_{Bn=0}$ with Bn are shown. Fis 10a–c demonstrate that $\overline{Nu}/\overline{Nu}_{Bn=0}$ reaches an asymptotic value (i.e. $1/\overline{Nu}_{Bn=0}$) corresponding to pure conduction heat transfer (i.e. $\overline{Nu}=1.0$) for a value of Bingham number $Bn_{\max}$ and $Bn_{\max}$ is found to increase with increasing AR. Eq. (42b) suggests that $\overline{Nu}/\overline{Nu}_{Bn=0}$ in the boundary-layer regime [22] is expected to show a self-similar behaviour with Bn^* provided the effects of $f_3(Pr, Bn)$ are not sufficiently strong to disturb this self-similar behaviour. On the other hand, in the parallel-flow regime (i.e. in the limit of $RaAR^3\rightarrow 0$) $(\overline{Nu}-1)/(\overline{Nu}_{Bn=0}-1)$ is expected to show self-similar behaviour with Bn^{**} provided the effects of $f_4(Pr, Bn)$ are not significant. The variations of $\overline{Nu}/\overline{Nu}_{Bn=0}$ with $Bn/AR^{1/4}$ for the $AR\geq 1$ cases for $Ra=10^4$, 10^5 and $10^6$are shown in Fig. 11a–c as boundary layer transport plays non-negligible role in $AR\geq 1$ cases for all the values of Rayleigh number considered in the present study. It can be seen from Fig. 10a–c that variations of $\overline{Nu}/\overline{Nu}_{Bn=0}$ with $Bn/AR^{1/4}$ collapse reasonably well for the $AR>1$ cases. However, it can be seen from Fig. 11a–c that the variation of $\overline{Nu}/\overline{Nu}_{Bn=0}$ with $Bn/AR^{1/4}$ for $AR=1.0$ does not collapse with the corresponding variations obtained for the $AR>1$ cases. Nevertheless, as shown in Fig. 11d–f, the variations of $\overline{Nu}/\overline{Nu}_{Bn=0}$ with $Bn/AR^{2/5}$ exhibit satisfactory collapse for all the $AR\geq 1$ cases considered here. As the scaling estimate given by Eq. (42b) provides only a rough guidance, the difference in the exponent n_B of aspect ratio AR (0.25 cf. 0.4) for the self-similar behaviour of $\overline{Nu}/\overline{Nu}_{Bn=0}$ with Bn/AR^{n_B} is perhaps not entirely unexpected. Moreover, the criterion for the onset of the boundary-layer regime ($Ra>4.4\times 10^4 AR^{-14/3}$, see Eq. (19)) does not provide a hard boundary between the intermediate flow and boundary-layer regimes [22] and it is possible that some of the attributes of intermediate flow regime exists for the $AR=1$ cases at the Rayleigh numbers considered here. This effect may also give rise to lack of collapse of the variation of $\overline{Nu}/\overline{Nu}_{Bn=0}$ with $Bn/AR^{1/4}$ for $AR=1.0$ cases with the corresponding variations obtained for $AR>1$ cases because the threshold Rayleigh number ($Ra>4.4\times 10^4 AR^{-14/3}$, see Eq. (19)) for the boundary-layer regime to exist in $AR>1$ cases is much smaller than that in $AR=1.0$ cases.

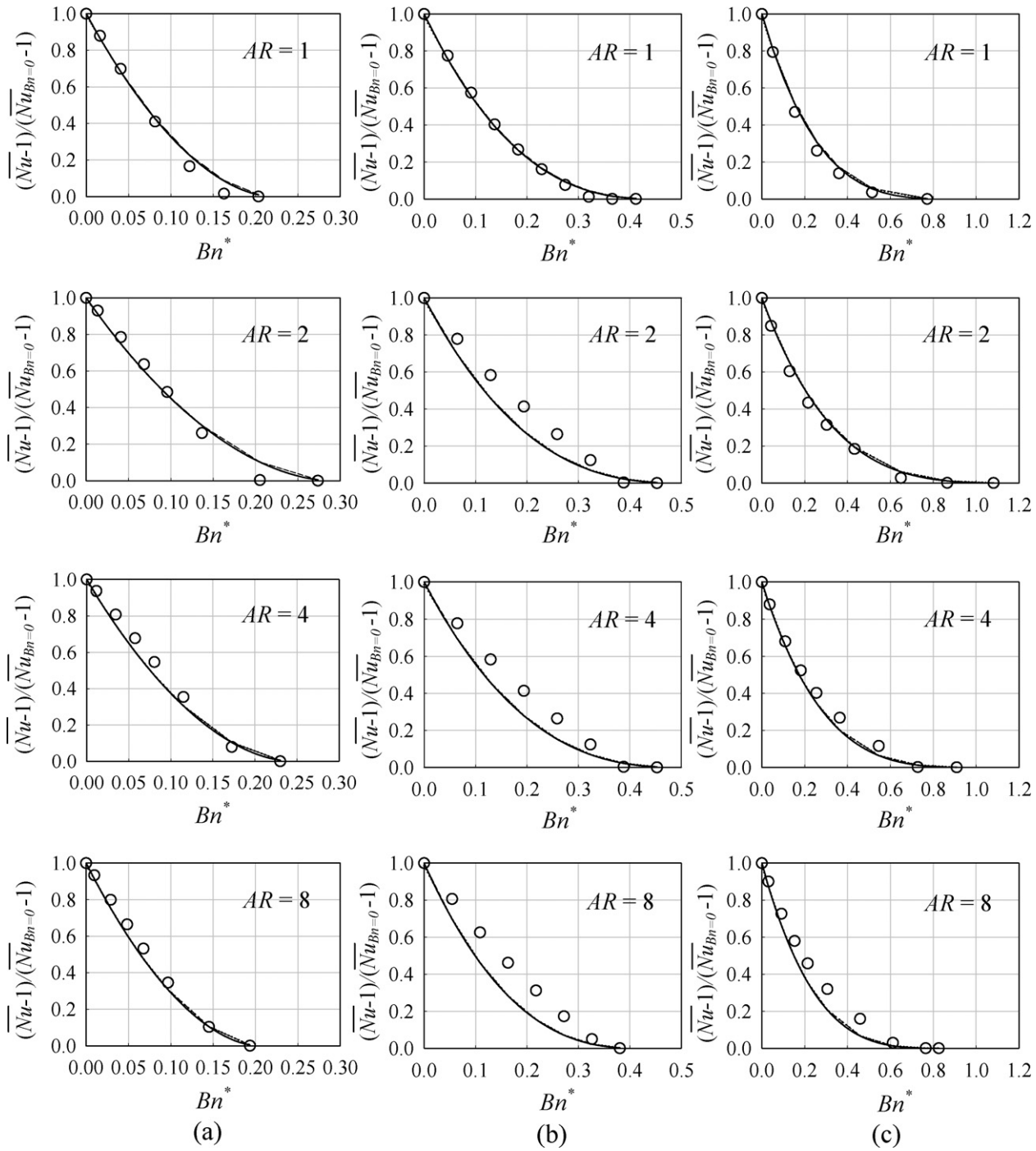

Fig. 13. Comparison of the predictions of the correlations given by Eq. (48) (—), Eq. (50) (- - -) and Eq. (51) (···) with simulation results (○) for $AR \geq 1$ cases at $Pr = 7$: (a) $Ra = 10^4$, (b) $Ra = 10^5$ and (c) $Ra = 10^6$.

The variations of $(\overline{Nu}-1)/(\overline{Nu}_{Bn=0}-1)$ with Bn/AR^2 for the $AR < 1$ cases are shown in Fig. 12 a and b for nominal Rayleigh numbers 10^5 and 10^6 respectively. The corresponding variation of $(\overline{Nu}-1)/(\overline{Nu}_{Bn=0}-1)$ at $Ra = 10^4$ is not shown here as $\overline{Nu}$ remains equal to unity for $AR = 0.125$ and 0.25 and attains the asymptotic value $\overline{Nu} = 1.0$ at a very small value of Bingham number for $AR = 0.5$ (see Fig. 10a). It can be seen from Fig. 12a and b that the variations of $(\overline{Nu}-1)/(\overline{Nu}_{Bn=0}-1)$ with Bn/AR^2 for different values of AR remain reasonably close to each other at a given value of nominal Rayleigh number Ra. The lack of complete collapse of $(\overline{Nu}-1)/(\overline{Nu}_{Bn=0}-1)$ with Bn/AR^2 is not unsurprising because Eq. (47b) was obtained based on the assumptions which are strictly valid only in the parallel-flow regime but many of the $AR < 1$ cases exhibit attributes of the intermediate flow regime (see Table 3) where the thermal boundary layers adjacent to the vertical walls start to influence the thermal transport.

Turan et al. [27] proposed a correlation for $\overline{Nu}$ for Bingham fluids based on numerical simulations of natural convection in a square enclosure with differentially heated side walls and, based on that analysis, $(\overline{Nu}-1)/(\overline{Nu}_{Bn=0}-1)$ can be written in the following manner for the boundary-layer regime:

$$\frac{\overline{Nu}-1}{\overline{Nu}_{Bn=0}-1} = \frac{2(1-Bn^*/Bn^*_{\max})^b}{Bn^*+\sqrt{Bn^{*2}+4}} \quad \text{when } \overline{Nu}_{Bn=0} > 1, \tag{48a}$$

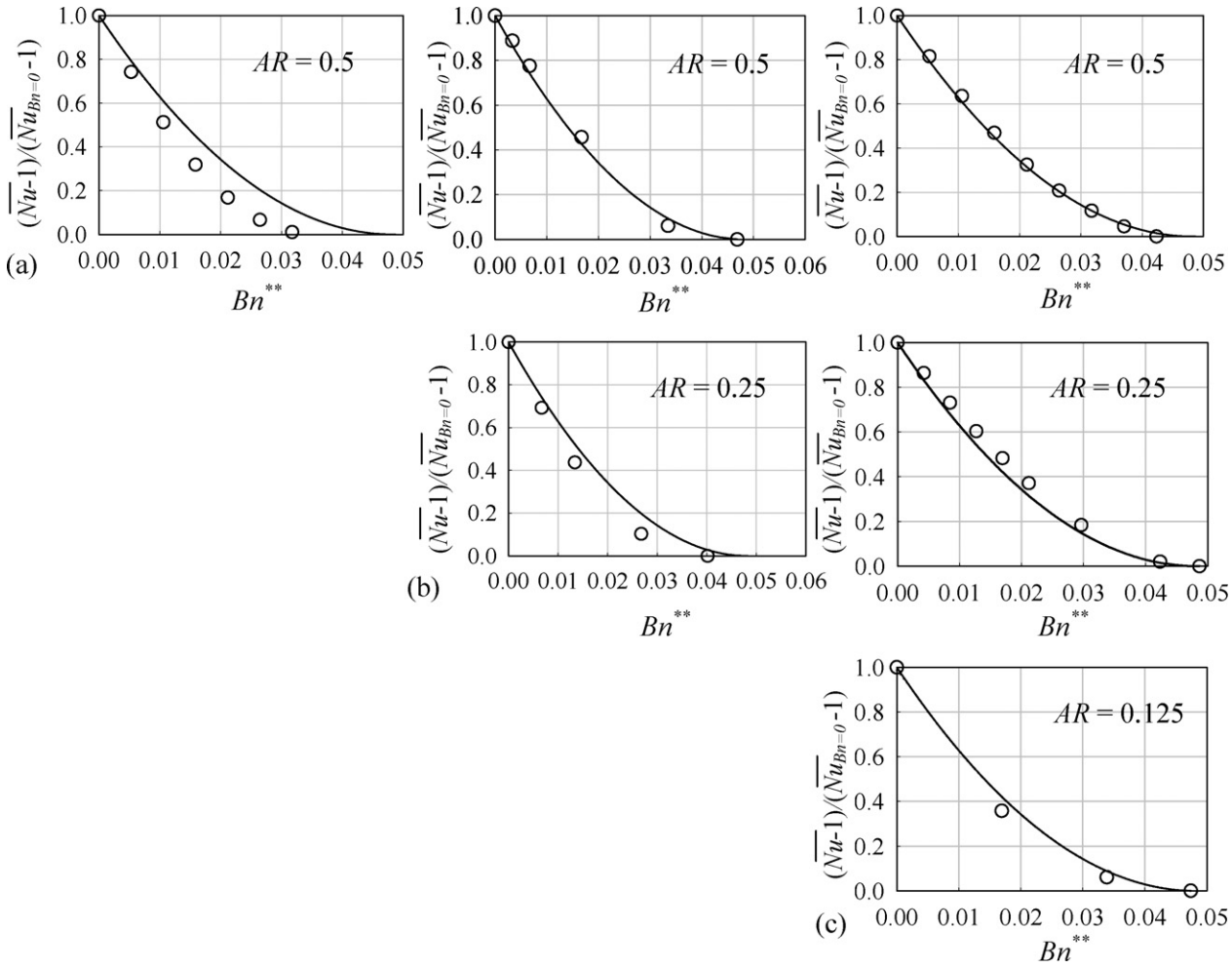

Fig. 14. Comparison of the predictions of the correlations given by Eq. (49) (—), Eq. (50) (- - -) and Eq. (51) (···) with simulation results (○) for $AR < 1$ cases at $Pr = 7$: (a) $Ra = 10^5$ and (b) $Ra = 10^6$.

and

$$\overline{Nu} = 1 \quad \text{when } \overline{Nu}_{Bn=0} = 1 \tag{48b}$$

where b is a model parameter and $Bn^*_{\max} = Bn_{\max}(Ra\,AR/Pr)^{-1/4}$ which can be expressed as:

$$b = 0.42Ra^{0.13}Pr^{0.12}, \tag{48c}$$

$$Bn^*_{\max} = CRa^{0.31}Pr^{-0.21}AR^{-0.25}, \tag{48d}$$

where the parameter C is given by:

$$C = 0.019 + 0.010erf(2AR - 2). \tag{48e}$$

According to Eq. (48d) the quantity $Bn_{\max}$ is directly proportional to $Ra^{0.56}/Pr^{0.46}$ which is sufficiently close to the $\sqrt{Ra/Pr}$ dependence of $Bn_{\max}$ as predicted by the scaling relation given by Eq. (35b). It can be seen from Fig. 13 that Eq. (48a) predicts $(\overline{Nu}-1)/(\overline{Nu}_{Bn=0}-1)$ satisfactorily (when b, $Bn^*_{\max}$ and C are expressed according to Eqs. (48c)–(48e) respectively) for the aspect ratio $AR \geq 1$ for nominal Rayleigh numbers $Ra = 10^4$, 10^5 and 10^6.

Based on Eq. (47b) a correlation for $(\overline{Nu}-1)/(\overline{Nu}_{Bn=0}-1)$ is proposed here for small values of aspect ratio (i.e. $AR \ll 1$) in the parallel-flow regime (i.e. $RaAR^3 \to 0$):

$$\frac{\overline{Nu}-1}{\overline{Nu}_{Bn=0}-1} = \left[1 - \left(\frac{1}{4.55}\right)^{-2} Bn^{**}\right]^2 \text{ when } \overline{Nu}_{Bn=0} > 1 \text{ and}$$
$$\overline{Nu} = 1 \text{ when } \overline{Nu}_{Bn=0} = 1. \tag{49}$$

It can be seen from Fig. 14 that the correlation given by Eq. (49) satisfactorily predicts $(\overline{Nu}-1)/(\overline{Nu}_{Bn=0}-1)$ for the $AR < 1$ cases representing the parallel flow and intermediate flow regimes of thermal transport.

The correlations given by Eqs. (48) and (49) can be combined to yield a single correlation for all the regimes of convection in rectangular enclosures with differentially heated side walls in the following manner:

$$\frac{\overline{Nu}-1}{\overline{Nu}_{Bn=0}-1} = \left[1 - \left(\frac{1}{4.55}\right)^{-2} Bn^{**}\right]^2 \exp(-m\,AR^{n_1})$$
$$+ \frac{2(1 - Bn^*/Bn^*_{\max})^b}{Bn^* + \sqrt{Bn^{*2}+4}}(1 - \exp(-m\,AR^{n_1})) \quad \text{when } \overline{Nu}_{Bn=0} > 1 \tag{50a}$$

and

$$\overline{Nu} = 1 \quad \text{when } \overline{Nu}_{Bn=0} = 1, \tag{50b}$$

where m and n_1 are given by

$$m = 4;\ n_1 = 8. \tag{50c}$$

Figs. 13 and 14 show that the combined correlation given by Eq. (50a) with model parameters given by Eq. (50c) captures the variations of $(\overline{Nu}-1)/(\overline{Nu}_{Bn=0}-1)$ satisfactorily for both the $AR \geq 1$ and $AR < 1$ cases considered here. This suggests that the expressions of $\overline{Nu}$ for Newtonian fluids (i.e. $\overline{Nu}_{Bn=0}$) as given by Eqs. (21), (23) and

(21) for $AR < 1$, $AR = 1$ and $AR > 1$ respectively can be used to predict the mean Nusselt number $\overline{Nu}$ for natural convection in Bingham fluids at the same nominal values of Ra and Pr using Eq. (50a) in the present configuration.

The correlation given by Eq. (50a) has two free parameters (i.e. m and n_1) and the number of free parameters can be reduced (to a single free parameter n_2) when an alternative combined correlation is constructed from Eqs. (48) and (49):

$$\frac{\overline{Nu}-1}{\overline{Nu}_{Bn=0}-1} = \left[\left[1-\left(\frac{1}{4.55}\right)^{-2} Bn^{**}\right]^{2/n_2} + \left[\frac{2(1-Bn^*/Bn^*_{\max})^b}{Bn^*+\sqrt{Bn^{*2}+4}}\right]^{1/n_2}\right]^{n_2} \quad \text{when } \overline{Nu}_{Bn=0} > 1, \tag{51a}$$

and

$$\overline{Nu} = 1 \quad \text{when } \overline{Nu}_{Bn=0} = 1. \tag{51b}$$

It has been found that for $n_2 = -0.02$ the correlation given by Eq. (51) predicts the behaviour of $(\overline{Nu}-1)/(\overline{Nu}_{Bn=0}-1)$ satisfactorily for both $AR \geq 1$ and $AR < 1$ and it can be seen from Figs. 13 and 14 that the prediction of Eq. (51) is comparable to that of Eq. (50) (in fact the predictions of Eqs. (50) and (51) cannot be distinguished from each other in Figs. 13 and 14). From the foregoing it can be concluded that the mean Nusselt number $\overline{Nu}$ for rectangular enclosures with differentially heated side walls filled with Bingham fluids can be predicted using the correlations given by Eqs. (50) and (51) provided appropriate correlations are used for the corresponding Newtonian case at the same nominal values of Rayleigh and Prandtl numbers.

5. Conclusions

In this study, the effects of aspect ratio ($=H/L$ where H is the enclosure height and L is the enclosure width) on the heat transfer characteristics of steady laminar natural convection of yield-stress fluids obeying the Bingham model in a rectangular enclosure with differentially heated side walls have been numerically studied. It is found that the mean Nusselt number $\overline{Nu}$ follows a non-monotonic trend with aspect ratio AR for a given set of values of the Rayleigh number and Prandtl number for both Newtonian and Bingham fluids. The effects of convection strengthen with increasing value of AR, whereas the strength of thermal conduction weakens with increasing AR. These competing effects of thermal convective and diffusive transports ultimately result in a non-monotonic variation of $\overline{Nu}$ with aspect ratio AR for both Newtonian and Bingham fluids. For very small values of aspect ratio the thermal transport remains predominantly conduction-dominated whereas the effects of convective transport remains predominantly responsible for heat transfer for large values of aspect ratio AR. The effects of weaker convective transport in Bingham fluids than in Newtonian fluids are reflected in the smaller values of the mean Nusselt numbers for Bingham fluids than those obtained in the case of Newtonian fluids with the same values of nominal Rayleigh number. The Nusselt number was found to decrease with increasing Bingham number, and, for large values of Bingham number (i.e. $Bn \geq Bn_{\max}$), the value of mean Nusselt number settled to unity (i.e. $\overline{Nu} = 1$) as the fluid flow effectively stops due to strong viscous stresses and heat transfer takes place principally due to conduction. The conduction-dominated regime occurs at higher values of Bn for increasing values of Ra (AR) for a given value of AR(Ra). The aspect ratio $AR_{\max}$ at which the maximum value of $\overline{Nu}$ is attained decreases with increasing value of Rayleigh number Ra in both Newtonian and Bingham fluids. The value of $AR_{\max}$ is found to increase with increasing value of Bingham number Bn for a given value of nominal Rayleigh number.

Finally, guided by a scaling analysis, the present simulation results are used to propose new correlations of $\overline{Nu}$ by accounting for aspect ratio AR effects in the case of convection in Bingham fluids. These correlations are shown to satisfactorily capture the variation of $\overline{Nu}$ with Ra, AR and Bn for all the cases considered in this study.

Acknowledgements

The visit of OT to Liverpool was funded by the European Union's Erasmus Lifelong Learning Programme and is hereby gratefully acknowledged.

References

[1] G.K. Batchelor, Heat transfer by free convection across a closed cavity between vertical boundaries ar different temperature, Q. J. Appl. Math. 12 (1954) 209.
[2] G. de Vahl Davis, Natural convection of air in a square cavity: A bench mark numerical solution, Int. J. Num. Methods Fluids 3 (1983) 249–264.
[3] A.F. Emery, J.W. Lee, The effects of property variations on natural convection in a square cavity, J. Heat Transfer 121 (1999) 57–62.
[4] S. Ostrach, Natural convection in enclosure, J. Heat Transfer 110 (1988) 1175–1190.
[5] J.W. Elder, Laminar free convection in a vertical slot, J. Fluid Mech. 23 (1965) 77–98.
[6] A.E. Gill, The boundary layer regime for convection in a rectangular cavity, J. Fluid Mech. 26 (1966) 515–536.
[7] M.E. Newell, F.W. Schmidt, Heat transfer by laminar natural convection within rectangular enclosures, Trans. ASME C: J. Heat Transf. 92 (1970) 159–167.
[8] S.H. Yin, T.Y. Wung, K. Chen, Natural convection in an air layer enclosed within rectangular cavities. Int. Heat Mass Transf. 21: 307-315.
[9] A. Bejan, Note on Gill's solution for free convection in a vertical enclosure, J. Fluid Mech. 90 (1979) 561–568.
[10] S.M. Elsherbiny, G.D. Raithby, K.G.T. Hollands, Heat transfer by natural convection across vertical and inclined air layers, ASME J. Heat Transfer 104 (1982) 96–102.
[11] Y. Lee, S. Korpela, Multicellular natural convection in a vertical slot, J. Fluid Mech. 126 (1983) 91–121.
[12] S. Wakitani, Formation of cells in natural convection in a vertical slot at large Prandtl number, J. Fluid Mech. 314 (1996) 299–314.
[13] P. Le Quéré, A note on multiple and unsteady solutions in two-dimensional convection in a tall cavity, Trans. ASME J. Heat Transf. 112 (1990) 965–973.
[14] S. Wakitani, Development of multicellular solutions in natural convection in an air-filled vertical cavity, Trans. ASME J. Heat Transf. 119 (1997) 97–101.
[15] Y. Zhao, D. Curcija, W.P. Gross, Prediction of multicellular flow regime of natural convection in fenestration glazing cavities, ASHRAE Trans. 103 (1) (1997) 1–12.
[16] R.L. Frederick, On the aspect ratio for which the heat transfer in differentially heated cavities is maximum, Int. Comm. Heat Trans. 26 (4) (1999) 549–558.
[17] B. Lartigue, S. Lorente, S.B. Bourret, Multicellular natural convection in high aspect ratio cavity: experimental and numerical results, Int. J. Heat Mass Transf. 43 (2000) 3157–3170.
[18] Y. Dong, Q. Zhai, Natural convection study in an enclosure with different aspect ratios, Int. J. Modern Phys. C 18 (12) (2007) 1903–1922.
[19] A.A. Ganguli, A.B. Pandit, J.B. Joshi, CFD simulation of heat transfer in a two-dimensional vertical enclosure, Chem. Eng. Res. Des. 87 (2009) 711–727.
[20] D.E. Cormack, L.G. Leal, J. Imberger, Natural convection in a shallow cavity with differentially heated end walls. Part 1. Asymptotic theory, J. Fluid Mech. 65 (1974) 209–229.
[21] D.E. Cormack, L.G. Leal, J.H. Seinfeld, Natural convection in a shallow cavity with differentially heated end walls. Part 2. Numerical solution, J. Fluid Mech. 65 (1974) 231–246.
[22] A. Bejan, C.L. Tien, Laminar natural convection heat transfer in a horizontal cavity with different end temperatures, J. Heat Transfer 100C (1978) 641–647.
[23] J. Imberger, Natural convection in a shallow cavity with differentially heated end walls. Part 3. Experimental results, J. Fluid Mech. 65 (1974) 247–260.
[24] A. Bejan, A synthesis of analytical results for natural convection heat transfer across rectangular enclosures, Int. J. Heat Mass Transfer 23 (1980) 723–726.
[25] A. Bejan, A.A. Al-Homoud, J. Imberger, Experimental study of high Rayleigh number convection in a horizontal cavity with different end temperatures, J. Fluid Mech. 109 (1981) 283–299.
[26] D. Vola, L. Boscardin, J.C. Latché, Laminar unsteady flows of Bingham fluids: a numerical strategy and some benchmark results, J. Comput. Phys. 187 (2003) 441–456.
[27] O. Turan, N. Chakraborty, R.J. Poole, Laminar natural convection of Bingham fluids in a square enclosure with differentially heated side walls, J. Non-Newtonian Fluid Mech. 165 (2010) 903–913.

[28] H.A. Barnes, The yield stress – a review or 'παντα ρει' – everything flows? J. Non-Newtonian Fluid Mech. 81 (1999) 133–178.
[29] E. Mitsoulis, Flows of viscoplastic materials: models and computations, in: D.M. Binding, N.E. Hudson, R. Keunings (Eds.), Rheology Reviews (2007) 135–178.
[30] E.J. O'Donovan, R.I. Tanner, Numerical study of the Bingham squeeze film problem, J. Non-Newtonian Fluid Mech. 15 (1984) 75–83.
[31] T.C. Papanastasiou, Flow of materials with yield, J. Rheol. 31 (1987) 385–404.
[32] R.J. Poole, B.S. Ridley, Development length requirements for fully-developed laminar pipe flow of inelastic non-Newtonian liquids, ASME J. Fluids Eng. 129 (2007) 1281–1287.
[33] H. Fellouah, C. Cestelain, A. Quld El Moctar, H. Peerhossaini, A numerical study of dean instability in non-Newtonian fluids, ASME J. Fluids Eng. 128 (2006) 34–41.
[34] R.J. Poole, R.P. Chhabra, Development length requirements for fully-developed laminar pipe flow of yield stress fluids, ASME J. Fluids Eng. 132 (3) (2010) 034501.
[35] S.V. Patankar, Numerical Heat Transfer and Fluid Flow, Hemisphere, Washington, DC, 1980.
[36] P.J. Roache, Quantification of uncertainty in computational fluid dynamics, Annu. Rev. Fluid Mech. 29 (1997) 123–160.
[37] B.M. Berkovsky, V.K. Polevikov, Numerical study of problems on high-intensive free convection, in: D.B. Spalding, H. Afgan (Eds.), Heat Transfer and Turbulent Buoyant Convection, Hemisphere, Washington, DC, 1977, pp. 443–455.
[38] W. Shyy, M.H. Chen, Effect of Prandtl number on buoyancy-induced transport processes with and without solidification, Int. J. Heat Mass Transfer 33 (1990) 2565–2578.
[39] E.E. Mitsoulis, T. Zisis, Flow of Bingham plastics in a lid-driven square cavity, J. Non-Newtonian Fluid Mech. 101 (2001) 173–180.
[40] A. Vikhansky, On the onset of Bingham liquid in rectangular enclosures, J. Non-Newtonian Fluid Mech. 165 (2010) 901–913.